Journal of South American Earth Sciences 128 (2023) 104422

Contents lists available at ScienceDirect

Journal of South American Earth Sciences

journal homepage: www.elsevier.com/locate/jsames

Paleoecological indicators of the highstand sea level on the Amazonian supralittoral until the last two millennia

Samuel Rodrigues Ribeiro [a,e,*], Roberto Célio Valadão [b], Makênia Oliveira Soares Gomes [c], Jonathas S. Bittencourt [d,e], Raquel Araújo Alves [a]

[a] Graduate Program of Geography, Institute of Geosciences, Federal University of Minas Gerais, MG, Brazil
[b] Geography Department, Institute of Geosciences, Federal University of Minas Gerais, MG, Brazil
[c] Biology Department, Minas Gerais State University, MG, Brazil
[d] Geology Department, Institute of Geosciences, Federal University of Minas Gerais, MG, Brazil
[e] Laboratory of Paleontology and Macroevolution (CPMTC), Institute of Geosciences, Federal University of Minas Gerais, MG, Brazil

ARTICLE INFO

Keywords:
Holocene sea-level change
Paleo-mangrove
Freshwater vegetation
Palynology
Itacuruçá flats

ABSTRACT

Holocene sea-level changes are ubiquitous worldwide. The relative sea levels (RSL) of the Northeast and Southeast littoral zones of Brazil were higher than the current level during the middle Holocene. It has been assumed that the RSL was stable since 7 ka BP in the North Brazilian littoral, particularly in the Amazonian coast. Based on a multiproxy approach (pollen content, $\delta^{13}C$, 14C-dating, and sedimentary and geomorphological features) applied to a sediment core obtained from the Amazonian supralittoral zone (>50 km away from the modern coastline), our study investigated the signatures of the RSL highstand in this region. The results show that the marine influence was more intense from 8410 to 1490 cal yr BP than that of the present. During this period, a mangrove community represented by *Rhizophora* and *Avicennia* established and thrived on the Itacuruçá tidal flat, probably due to post-glacial sea-level rise, which surpassed the present level during the middle Holocene. The mangrove population declined after 1490 cal yr BP, while freshwater vegetation developed, with the dominance of various associations of taxa. The sudden deposition of organic debris in the sedimentary record is consistent with the decrease in mangrove communities. This pronounced environmental change is possibly related to the reduction of the RSL, which reached the present-day position before the last millennium. Climate influence has not been recognized as significant in this process. Irrespective of the curve model showing the position or values from the RSL and related causes, this investigation addresses the indicators of this phenomenon. The results presented here suggest that understanding the variable trends of the Late Holocene RSL and their influence on paleoecological dynamics and paleogeographical evolution requires further advancement.

1. Introduction

Sea-level changes occur worldwide over a broad range of spatio-temporal scales. As a ubiquitous phenomenon in coastal regions, these changes have been recognized through geomorphology (Kelletat, 2019), strata stacking patterns of the sedimentary rocks (Allen and Posamentier, 1993; Dalrymple et al., 1994; Ghandour et al., 2021), systems of coastal valley drowning and river connectivity (Evans and Prego, 2003; Galili et al., 2005), and littoral spatial dynamics of ecosystems (Cameron and Palmer, 1995; Yao and Liu, 2017). The growing interest in sea-level changes has fostered technical (e.g., satellite-based radar altimeter and tidal gauge of high-precision) and methodological advances in the study and interpretation of paleo-sea levels. Gathering evidence of these events helps to understand the structure of shore landscapes under distinct characteristics (geological, geomorphological, biological, and hydrological), which allows for the development of a more realistic paleogeographic framework. This provides support for the accuracy of modeling predictions of relative sea level (RSL) rise from a future perspective (Dayan et al., 2021; Sampath et al., 2015).

Systematic investigations focusing on reconstructing the paleo-sea level along the Brazilian coast have been conducted based on organic content, topographical indicators, and 14C chronology of the seashore sediments (Angulo et al., 2006; Bezerra et al., 2003; Boski et al., 2015; Castro et al., 2014; Martin et al., 2003; Suguio et al., 2013; Tomazelli,

* Corresponding author. Laboratory of Paleontology and Macroevolution (CPMTC), Institute of Geosciences, Federal University of Minas Gerais, MG, Brazil.
E-mail address: ribeiro.samr@hotmail.com (S.R. Ribeiro).

https://doi.org/10.1016/j.jsames.2023.104422
Received 5 May 2022; Received in revised form 19 April 2023; Accepted 28 May 2023
Available online 4 June 2023

1990). For example, in the eastern and southeastern littoral zones, these investigations revealed that the sea level was previously higher than that of the present because of the influence of the interglacial period (middle Holocene), with a late-Holocene trend of RSL decline until the current level (Angulo et al., 2006; Angulo and Lessa, 1997; Bezerra et al., 2003; Boski et al., 2015; Dominguez et al., 1990; Suguio et al., 2013). The paleo-sea level of the Amazon has been studied in terms of pollen analysis and sedimentary facies, as well as with $\delta^{13}C$, $\delta^{15}N$, C/N, and Holocene radiocarbon chronology. These multi-proxy investigations have identified that RSL reached its current level between 7000 and 5000 yr BP and has remained stable since (e.g., Behling et al., 2001; Behling and da Costa, 2000; Cohen et al., 2005; Rossetti et al., 2008; Vedel et al., 2006).

The interglacial sea level of the Amazon could have exceeded the present level during the middle Holocene, which is supported by the peat deposits cropping out at the Maratauíra riverbank, 180 km from the coastline. The development of peat deposits could be attributed to paleo-mangrove demise after the RSL declined to the current level. In addition, a present-day mangrove fringe represented mainly by *Rhizophora* on the estuarine landscape, otherwise dominated by freshwater vegetation, can be evidence of the post-glacial sea-level rise that affected this region (Ribeiro and Valadão, 2021, 2020). If mangroves previously occupied this region, then it is plausible that the relative sea level could have been higher than that of the present-day in northern Brazil.

Mangrove forests are unique ecosystems because of their physiological adaptations to harsh saline environments (Mukherjee et al., 2015; Spalding et al., 2010). Mangroves grow on mudflats between mean sea level and high spring tide in tropical and sub-tropical shorelines worldwide (Polidoro et al., 2010). Their growth depends on temperature, tidal inundation frequency, and mud sediment supply (Lugo and Snedaker, 1974). Kodikara et al. (2018) demonstrated that optimal growth and productivity rates in this forest can occur at concentrations ranging from 15 to 17 PSU due to the regulation of leaf water, osmotic potentials, and stomatal conductance, which present better physiological performances under moderate salinity.

Mangrove community dynamics are also related to changes in sea level, as they migrate landward with a rise in sea level, and seaward when the level declines (Blasco et al., 1996; Gilman et al., 2008). Some investigations have demonstrated the complex relationship among the growth, spatial, and temporal fluctuations and demise of mangroves on coastal interfaces conditioned by freshwater (Aziz and Khan, 2001; Naidoo, 1985). Considering the mangrove responses to sea-level changes, the marine influence can be traced based on the spatiotemporal dynamics, in this case, using a field away from the shoreline.

In northern Brazil, outside the Amazonian coast, there is little evidence of the effects of Holocene marine incursion on the supralittoral sector (>50 km from the modern shoreline). The most expressive is based on the geomorphological features of the drowned valleys on the sheltered coast of Marajó Island, approximately 250 km west of our study area (e.g., Barbosa et al., 1974). However, despite some geomorphological relevance, such evidence has been criticized because of the absence of physical significance, lack of analogous proximal indicators for correlation, and mainly the scarcity of chronological and bio-stratigraphical data. Therefore, these issues contributed to assigning the possible Holocene transgression to a hypothetical scenario.

To date, no comprehensive study has examined the micropaleontological content of the Amazonian supralittoral to detect possible Holocene marine influences (or constrain the sea-level rise), although this area is a sensitive and potentially untapped region that could explain the RSL trends based on ecological history. Its distant location enables the tracing of marine incursion influences outside the modern coastline, which is typically well-researched. Therefore, we studied a core retrieved from a supratidal environment of southeast Abaetetuba city, Pará River Upper Estuary, northern Brazil, to detect marine transgressive events. The pollen content and sedimentary features of the MLT2 core were combined with $\delta^{13}C$, ^{15}N, organic matter C/N, and chronological data to propose a paleoenvironmental overview of the Amazonian supralittoral evolution occurring between the middle and late Holocene.

2. Study area

The Itacuruçá estuarine plain river is located in the south-southwest part of Abaetetuba, 180 km from the modern coastline. This sector comprises the Pará River Upper Estuary (ESP), classified as semidiurnal micro-to mesotidal (Ribeiro and Valadão, 2021). The Tocantins River is the main fluvial body of the ESP (Fig. 1a), which has an approximate discharge of 10,900 $m^3\ s^{-1}$ (ANA, 2019; Prestes et al., 2020). This high fluvial discharge prevents the ESP from experiencing saline influence (<0.5); thus, Itacuruçá and other water bodies from the ESP have been defined as tidal rivers, that is, their hydrodynamics are controlled by the tide. However, the large freshwater input results in virtually non-existent salinity levels (Ribeiro and Valadão, 2021).

The geomorphology of the area consists mainly of lowlands that shelter wide valleys and numerous estuaries, resulting in a jagged inshore setting (Fig. 1a). Extensive islands occur alongside the littoral zone, mainly between the Amazon, Pará, and Tocantins river mouths, which are part of a geologically young system, often assigned to the Late Pleistocene-Holocene (Barbosa et al., 1974). These fluviomarine plains constitute the main local morphological units, with elevations of up to 5 m above the local reduction level (Fig. 1c). The region is subdivided into three zones: subtidal (<1 m), intertidal (1–3 m), and supratidal (3–5 m). However, because of the spatial scale adopted in this study, only the central unit, that is, the fluviomarine plain, can be represented by mapping. The fluviomarine plain is partially prone to regular flooding by the mesotidal regime, with spring tides reaching up to 3.78 m (Ribeiro and Valadão, 2021).

The vegetal cover includes pioneer formations in the subtidal zone, composed mainly of *Montrichardia linifera*, *Mauritia flexuosa*, *Machaerium lunatum*, and *várzea* vegetation, dominated by terrestrial trees that are tolerant to flooding, such as *Euterpe oleracea* and *Pterocarpus amazonicus*, which occupy the intertidal zone. In contrast, the supratidal zone is mainly covered by *Virola surinamensis*, *Swartzia polyphylla*, *Hevea brasiliensis*, and *Calycophyllum spruceanum*. The Terra Firme, a morphological unit not subjected to tidal influence, occurs upstream of the study area. This unit varies between 5 and 15 m, but in the insular complex (Fig. 1b and c), the Terra Firme does not exceed 8 m. Its vegetation cover consists mainly of *Vouacapoua americana*, *Dipteryx odorata*, and *Manilkara huberi* (Ribeiro and Valadão, 2021, 2020). These vegetation groups are related to dense alluvial ombrophilous forests (Fig. 1b). The climate is classified as typical warm and humid tropical. The influence of seasonality of the Intertropical Convergence Zone (ITCZ) results in a characteristic climate with two seasons (Souza-Filho et al., 2009), a rainy season that occurs between January and July and a drier season prevailing for the rest of the year (July to December). The total precipitation averages 2700 mm per year, and the mean annual temperature is 27 °C (FAPESPA, 2016).

Miocene rocks and quaternary sedimentary deposits characterize the geology of the area. The Pirabas/Barreiras formations consist of Miocene limestones, laminated mudstones, and calciferous sandstones (Ferreira, 1977). The Barreiras Formation (Miocene/Middle Miocene) consists of conglomerates, sandstones, and claystones (siliciclastic non-fossiliferous) (Góes et al., 1990; Rossetti et al., 1989). Eolian and fluvial-estuarine sandy and muddy sediments of the Late Pleistocene and Early Holocene overlie the Barreiras Formation. These sediments are termed post-Barreiras deposits (Tatumi et al., 2008). Post-Barreiras deposits are often capped by debris-lateritic deposits (?Pleistocene), distributed in riverbank outcrops in the study area, related to the fluvial environment, and further overlain mainly by estuarine Holocene deposits (Ribeiro, 2022). A large part of this region is governed by neotectonic forces, whose major structures control the river's course, creating accommodation space and displacing Holocene deposits,

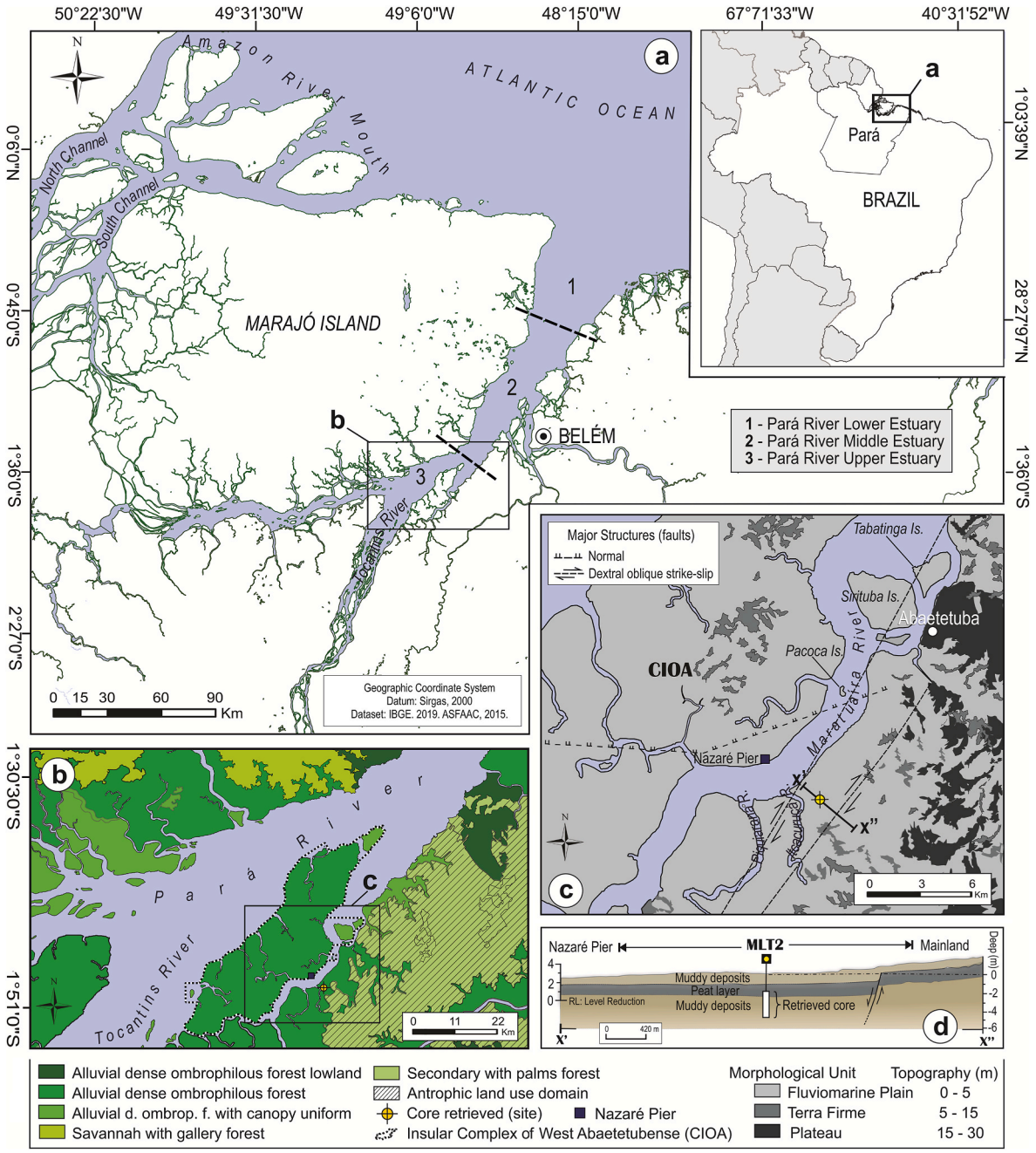

Fig. 1. Study area on the northern coast of the state of Pará detached from Brazilian territory (a). Regional distribution of vegetation (b) followed by main morphological features, with tectonic structures and sampling site at the Itacuruçá estuarine plain (c). Note the integrated profile sketch (sedimentary setting, topography, and reduction level), illustrating the MLT2 core position beneath the present-day surface (d).

affecting even the last millennium-deposited strata (Ribeiro, 2022) (Fig. 1c and d).

3. Materials and methods

3.1. Remote sensing

The cartographic database was obtained from the Brazilian Institute of Geography and Statistics (IBGE) (http://www.ibge.gov.br/geociencias/downloads-geociencias). The integrated approach of this study consisted of combined morphostructural and topographic data, which were analyzed using remote sensing products, including images from ALOS-PALSAR radar data (http://search.asf.alaska.edu). The dataset obtained consisted of radiometric terrain corrected (RTC) images with HH polarization mode (RT1) and 12.5 m resolution, to produce a high-resolution digital elevation model (DEM). The DEM was geometrically corrected, filtered, and patterned using SIRGAS 2000 as the reference, and used to generate the local topographical profile. The DEM was used to extract lineaments based on the visual analysis and correlated with the features previously reported by the Geological Survey of Brazil (CPRM) (http://geobank.sa.cprm.gov.br). After fieldwork, other minor lineaments were manually fixed and vectorized on the DEMs. In addition to radar data, cartographic datasets consisting of shapefiles from the natural environment (hydrography, geology, geomorphology, and vegetation) were obtained from the same IBGE repository. After fieldwork, the remote sensing products were manually interpreted and vectorized in detail. All processing and analyses were performed in a GIS environment (ESRI ArcGIS software v. 10.2®).

3.2. Fieldwork and sample processing

One sediment core was retrieved during fieldwork in January 2019. The sampling site consisted of a supratidal flat near the entrance of the Itacuruçá River. The MLT2 core (1°48'11.47″S, 48°56'39.66″W) was approximately 463 m from this river (Fig. 1c). The drilling reached a depth of 550 cm, and the retrieved core corresponded to the deepest part of the sample. The MLT2 had a depth of 280 cm and was collected using Russian corer equipment. The top of the MLT2 core (0 cm depth) was 2.70 cm beneath the surface (see sketch illustrating the MLT2 sampling position in the sedimentary context, Fig. 1d). The core topography was defined based on the local reduction level measured in the Nazaré Pier, localized on the Insular Complex of West Abaetetubense (CIOA), following the procedures of Ribeiro and Valadão (2021) (Fig. 1c and d). The Global Position System (GPS) determined the core geographical coordinates using SIRGAS 2000 as the reference. In addition to MLT2 core, at different locations along the study area, visual analysis of outcrops was performed, including morphological and geobotanical unit descriptive surveys.

3.3. Facies description core

Facies analysis was performed, including a description of color (Munsell Soil Color Charts, 2009), texture, and structure, following the methods of Walker (1992). Macroscopic analysis of sediments was also conducted by recording sandy sediment size, sorting, and rounding. The sedimentary facies were codified according to Miall (1978). Finally, the MLT2 core profile was integrated into pollen data and divided into facies associations that were genetically related and had identical environmental significance; therefore, they were indicative of a particular sedimentary environment (Reading, 1996). This is critical for achieving paleoenvironmental evolution models (Dalrymple and Choi, 2007).

3.4. Pollen and spore analysis

Fifty-six 1 cm^3 samples were retrieved at 5 cm intervals throughout the MLT2 core for pollen analysis. All samples were prepared using standard pollen analytical techniques, including KOH-10% and acetolysis (Erdtman, 1960). The sample residues were mounted on slides in a glycerin gelatin medium. Pollen and spores were identified by comparison with reference collections of approximately 4000 Brazilian forest taxa and various pollen keys (Colinvaux et al., 1999; Absy, 1975; Roubik and Moreno, 1991), based on the reference collection of the Paleontology and Macroevolution Laboratory, Federal University of Minas Gerais. Pollen and spore data were presented as percentages of the total terrestrial pollen sum in pollen diagrams. The taxa were grouped according to the source: mangroves, trees, shrubs, palms, herbs, and ferns. The software TILIA and TILIAGRAF were used to calculate and plot the pollen diagram (Grimm, 1987). CONISS was used for cluster analysis of pollen taxa, permitting the zonation of the pollen diagram.

3.5. Isotopic and elemental analysis

Isotopic analysis ($\delta^{13}C$, $\delta^{15}N$) has the potential to identify changes in the sources of Organic Matter (OM) for each depositional environment, including the relationship between C/N (vvv). For instance, the C3 terrestrial plants show $\delta^{13}C$ values between −32‰ and −21‰ and C/N ratio >12, while C4 plants have $\delta^{13}C$ values ranging from −17‰ to −9‰ and C/N ratio >20. In C3-dominated environments, freshwater algae and marine algae have $\delta^{13}C$ values between −25‰ and −30‰ and −24‰ to −16‰, respectively, while algae present $\delta^{13}C$ values ≤ 16‰ on the C4-dominated environments (Haines, 1976; Deines, 1980; Meyers, 1994). On the other hand, $\delta^{15}N$ is used as an indicator of organic matter sources and paleoproductivity; $\delta^{15}N$ > 10.0‰ indicate aquatic OM as the source (phytoplankton), while terrestrial vascular plants present an average of 0‰ (Meyers, 1994; Thornton and McManus, 1994). Hence, the preserved elemental and isotopic compositions from sediments used in tandem ($\delta^{13}C$, $\delta^{15}N$, and C/N) allow tracing of the sources of MO in coastal deposits.

A total of 18 samples (2–20 mg) were collected from the core at intervals of approximately 15 cm. To measure TOC and TN, the sediment samples were treated with 4% hydrochloric acid to remove carbonate, washed with distilled water until the pH reached 6, dried in an oven at 50 °C, and finally homogenized. Each sample (0.50 mg) was added to a tin capsule and packed. The samples were analyzed for total organic carbon (TOC) and total nitrogen (TN) by isotope ratio mass spectrometry (IRMS Hydra 20-20), interfaced with an automatic N and C analyzer (ANCA GLS) coupled to an automatic sampler (222 XL Liquid Handler, Gilson) at the Stable Isotope Laboratory of the Center for Nuclear Energy in Agriculture (CENA/USP). The results are expressed as a percentage of dry weight, with analytical precisions of 0.09% (TOC) and 0.07% (TN). The $\delta^{13}C$ and $\delta^{15}N$ results were expressed in per mille (‰) with respect to the VPDB and N2 standards, respectively, with a precision of 0.2‰. The elemental results were used to calculate the C/N ratio (weight/weight) of all samples. The determination of organic matter sources, such as C3 and C4 terrestrial plants and marine and freshwater algae, will be environmental-dependent with a specific $\delta^{13}C$, $\delta^{15}N$, and C/N composition (Lamb et al., 2006; Meyers, 1997; Thornton and McManus, 1994).

3.6. Radiocarbon dating

Four bulk samples (approximately 10 g each) along the MLT2 core were selected for dating. This selection was based mainly on the deposit discontinuity, sediment nature, texture, and color. The samples were examined and subjected to DirectAMS. A chronological framework for the sedimentary samples was provided by accelerator mass spectrometry (AMS) dating at DirectAMS Laboratory (Bothell). Radiocarbon ages were normalized to a $\delta^{13}C$ value of 25‰ VPDB and reported as calibrated years (cal yr BP, 2σ) using CALIB 8.2 and the SHCal20 curve (Hogg et al., 2020). The dates are reported in the text as the median of the range of calibrated ages (Table 1).

4. Results

4.1. Radiocarbon dates and sedimentation rates

The radiocarbon ages calibrated are shown in Table 1 and Figs. 2 and 3. The sample from the core bottom (280 cm) registered 8389–8419 cal yr BP, followed by 6693–6732 cal yr BP at a depth of 162 cm, 3402–3430 cal yr BP at a depth of 85 cm, and 1475–1526 cal yr BP near the MTL2 top, at the peat basal (35–37 cm). The rates of sedimentation were estimated from the thickness of the deposits and their numerical ages, presenting 0.67 (280–162 cm), 0.25 (162–085 cm), and 0.23 mm/yr (85–37 cm) (Fig. 2). No age inversions were observed.

4.2. Core facies description

The sediment MLT2 core consisted primarily of mud with internal structures that include a heterolithic lenticular, and peat deposits. The peat deposits were mainly well-decomposed fibers rather than younger vegetable roots. Facies were identified based on internal sedimentary structures, organic content, sediment texture and color, and contact relationships. Pollen and spore records, and $\delta^{13}C$, $\delta^{15}N$, and C/N values were added to the facies structures, allowing for two facies associations: tidal flat (A) and swamp mixed estuarine flat (B). The characteristics of each of these associations are summarized in Table 2.

4.3. Facies Association A (tidal flat)

This unit was almost fully cored into the MLT2. It occurs along the interval 280–38 cm in the core studied and comprises deposits of

Table 1
Sediment samples selected for radiocarbon dating with laboratory number, code core/depth,^{14}C yr BP and calibrated (cal) ages.

Laboratory number (D-AMS)	Sample	Depth beneath the surface (cm)	Depth Core (cm)	Age BP	Ages (Cal yr BP, 1σ)	Ages (Cal yr BP, 2σ)	Median Probabilily
044,419	MLT2–peat basal	287–290	35–37	1633 ± 30	1475–1526	1448–1530	1490
050,411	MLT2	340	85	3260 ± 23	3402–3430	3387–3453	3422
046,399	MLT2	447	177	5902 ± 28	6693–6732	6630–6747	6690
038,504	MLT2	550	280	7661 ± 38	8389–8419	8374–8452	8410

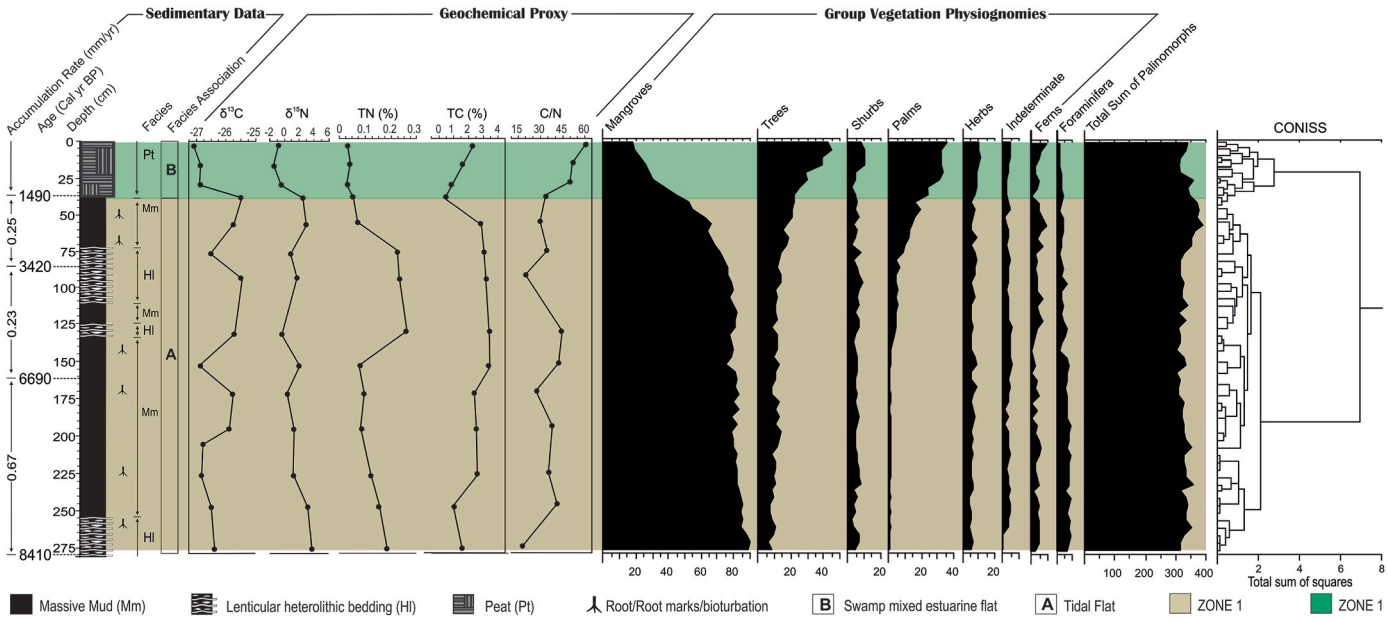

Fig. 2. Sediment core framework, integrated to geochemical results, C14 ages, and pollen diagram with percentages of the physiognomic group ecological.

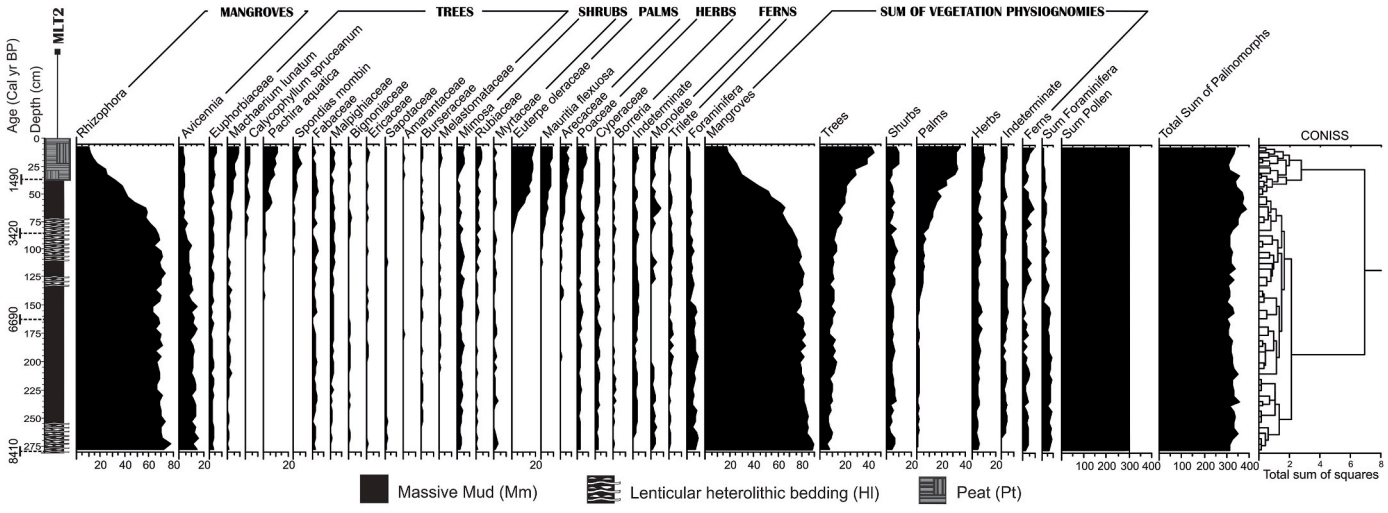

Fig. 3. Pollen diagram of the core MLT2, with percentages of the most frequent pollen taxa, samples age, and cluster analysis.

organic-rich mud with fine sands well sorted. Radiocarbon dates indicate that accumulation occurred between 8410 cal yr BP and 1490 cal yr BP (Fig. 2). Their facies element structures consist of massive mud (Mm) and lenticular heterolithic bedding (Hl). The latter has a subordinate (31%) without continuous occurrence, representing 75 cm of 242 cm in this succession (Figs. 2 and 3). The Mm (structureless), may occasionally present planar and parallel laminated mud. Locally, this deposit exhibits gray scattered pigmented mottles and bioturbation features such as woody roots and root marks (Fig. 5b). The heterolithic lenticular-bedding facies, in turn, is characterized by oscillation ripples of millimeter-thickness fine sand lenses, which may gradually enlarge to form sand waves. Altogether, these bedforms are linked with a low

Table 2
Facies associations identified along the MLT2 core according to sedimentary characteristics, pollen and geochemical data.

Facies Association	Facies description	Pollen dominance	Geochemical data	Paleoenvironment
A	Massive mud (Mm), olive-brown, gray to very dark gray and black; parallel lamination mud can be present. Heterolithic lenticular deposits (Hl) olive-brown, greenish to gray to dark gray and black. Lenticular structures rhythmic interbedded in variable proportions of sand; these deposits contain woody roots and root marks.	Mangrove	$\delta^{13}C = -25.5$ to -26.8‰ $\delta^{15}N = -1$ to 4‰ C/N = 15–45 TOC = 0.9–3.4% TN = 0.07–0.27% %	Tidal Flat
B	Peat deposits (Pt), black, brown-reddish, and black to dark-gray, well-decomposed, with mud drapes. Locally, they present abundant bioturbations and dwelling structures produced by the benthic fauna, which are easily recognized.	Trees and palms	$\delta^{13}C = -25.5$ to -27.2‰ $\delta^{15}N = -0.9$ to 2.7‰ C/N = 30–62 TOC = 0.4–2.3% TN = 0.02–0.05%	Swamp mixed estuarine flat

energy flow environment to deposition from suspension (Mm), with alternating traction force to sand lens deposition (Hl) (Fig. 2).

Pollen assemblages of Association A allowed the identification of 21 pollen taxa. This zone was dominated by mangrove pollen (62–88%) and was composed of *Rhizophora* (42–86%) and *Avicennia* (4–16%). The pollen spectra also included ecological groups of trees (6–22%) and shrubs (4–9%), mainly Euphorbiaceae (3–7%), Fabaceae (2–6%), Malpighiaceae (1–5%), *Mimosa* (3–11%), Rubiaceae (0–9%), Bignoniaceae (0–4%), and Burseraceae (0–4%). The palm ecological group appeared with percentages <18%, and herb pollen comprised <11%. Palms are represented by *Euterpe oleraceae* (0–15%) and *Mauritia flexuosa* (0–8%), while Poaceae (3–8%), Cyperaceae (2–6%), and *Borreria* (0–3%) represent the herbs. Trilete and monolete ferns formed between 1 and 11%, and foraminifera between 3 and 10% in this zone (Figs. 2 and 3). Organic matter $\delta^{13}C$ ranged from −26.8 and to −25.5‰ (mean −26.2‰), whereas $\delta^{15}N$ varied between −1 and 4‰ (mean 2.5‰). The TOC results ranged between 0.9 and 3.4% (mean = 2.1%), the TN values varied from 0.07 to 0.27% (mean = 1.8%), and the minimum and maximum C/N values were 15 and 45, respectively (Fig. 2, Table 2).

4.4. Facies Association B (swamp mixed estuarine flat)

Association B occurred between 38 and 0 cm in the uppermost part of the core, representing 13.6% of the MTL2 (Fig. 2). It was formed of well-decomposed peat deposits with internal organic muddy drapes. This unit was deposited after 1490 cal yr BP. Besides the sample at the core (Supplementary P1), this peat presented good quality outcrops on the river bank, yielding almost continuous exposure through the Maratauíra and Maiauatá rivers (Supplementary P2). In addition, the presence of rivers that enter estuarine tidal flats allow for the analysis and inference of their spatial distribution, such as the records at the Furo Grande and Maracapucu-Miri localities of the CIOA. Accordingly, the upper contact of the peat with muddy deposits (not retrieved) has been recognized as abrupt to gradual, mainly based on the outcrop scale (Supplementary P2).

The lowest contact relation was inferred from cores drilled previously (Supplementary P1). The drilled cores revealed a predominantly abrupt contact between the peat and the underlying unit. The latter is often muddy but encompasses heterolithic deposits consisting of fine sand. The advancement of the survey in this region suggests a correlation between peat layers, indicating a widespread geographical distribution throughout the supralittoral sector. Such elements lead us to assume that peat formation is related to common depositional processes, with a paleoenvironmental significance assigned to swamp mixed estuarine flats.

Pollen analysis revealed the predominance of trees (22–45%), palms (18–38%), and mangroves (19–55%). Trees mainly consisted of Euphorbiaceae (4–14%), *Pachira aquatica* (4–11%), *Machaerium lunatum* (2–9%), *Spondias mombin* (1–7%), Malpighiaceae (0–7%), and *Calycophyllum spruceanum* (0–5%), whereas the palm group as mainly characterized by *Euterpe oleraceae* (15–20%), *Mauritia flexuosa* (8–19%), and Arecaceae (4–8%). Mangrove pollen was represented by *Rhizophora* (9–35%) and *Avicennia* (4–8%). Herb groups had low percentages (<9%). Ferns (1–10%) were represented by monolete and psilate trilletes, and foraminifera ranged from 3 to 6% (Figs. 2 and 3). The $\delta^{13}C$ and $\delta^{15}N$ values are between −27.2 and approximately −25.5‰ (mean −26.4‰) and −0.9 and 2.7‰ (mean 1.8‰), respectively. The C/N values occur between 30 and 62, and the C/N values were between 30 and 62, and the TOC values varied between 0.4 and 2.3% (mean = 1.4%), and TN values were stable at approximately 0.03% (Fig. 2, Table 2).

5. Discussion

5.1. The history of mangrove establishment in the supralittoral region

Pollen preserved in the lower part of the MLT2 core indicated an intertidal environment occupied by mangroves. This ecosystem has a growth performance in brackish water, tolerating high salinity (Ball, 1998; Spalding et al., 2010). For example, *Avicennia* demonstrates extreme salt tolerance, and *Rhizophora* exhibits relatively high salt tolerance (Jayatissa et al., 2008; Kodikara et al., 2018). The trigger for the initial conditions for mangrove development in this sector was likely the post-glacial sea level rise through saline input. The dominance of *Rhizophora*, with the genus *Avicennia* subordinate along the 268 cm (280–40 cm), suggests a brackish estuary with a biologically consolidated halophyte community (Figs. 2, 3, 4–I and 5a).

According to Panapitukkul et al. (1998), *Avicennia* represents a pioneer species; it develops first on mudflats that provide resistance to waves and currents. Consequently, successional colonization by other species, especially *Rhizophora* and *Brugeria*, which occupy available space, results in a mangrove zonation pattern (Thampanya, 2006). Thus, this mangrove is represented mainly by *Rhizophora*, while *Avicennia* suggests a climax stage of mangrove forest in the estuarine landscape. In

addition, the frequent presence of the foraminifera genus *Ammonia,* which is typically related to shallow nearshore areas, estuaries, and tidal swamps (e.g., Murray and Alve, 1999; Long et al., 2006), indicates that these conditions existed and followed alongside the mangrove community. The radiocarbon dates show that mangrove has been established in the supralittoral region for the last 8410 cal yr BP (Figs. 2 and 4–I).

The mechanism for the shoreside landscape setting was mainly sea-level changes. Estuarine bodies along global coastlands altered in relation to Holocene sea-level rise (Wolanski and Elliott, 2015). The marine incursion affected these morphologies and produced embayments within pronounced valleys inherent to the Pleistocene sea-level fall (Evans and Prego, 2003). This region shares an analogous palaeogeographical history, in which the Maratauíra River is an unfilled incised valley that opened during the Late Pleistocene-Early Holocene, driven by tectonic mechanisms coupled with glacial sea-level decline (Ribeiro, 2022). Consequently, the marine incursion reached the supralittoral region, producing rias and forming a variety of estuarine sub-environments with more expansive tidal flats. The transgressive event marks the gradual drowning of numerous fluvial features landward, extending the marine realm 180 km beyond the modern coastline (Fig. 4–I–II).

Deposits are dominantly muddy and frequently interbedded with layers and lenses of well-sorted, very fine-grained sands constituting MLT2 core Zone 1 (Fig. 2). Sedimentary structures with alternating beds/laminae of sand and mud are primarily formed in tidal settings (Daidu et al., 2013) because slack tides favor mud deposition in very

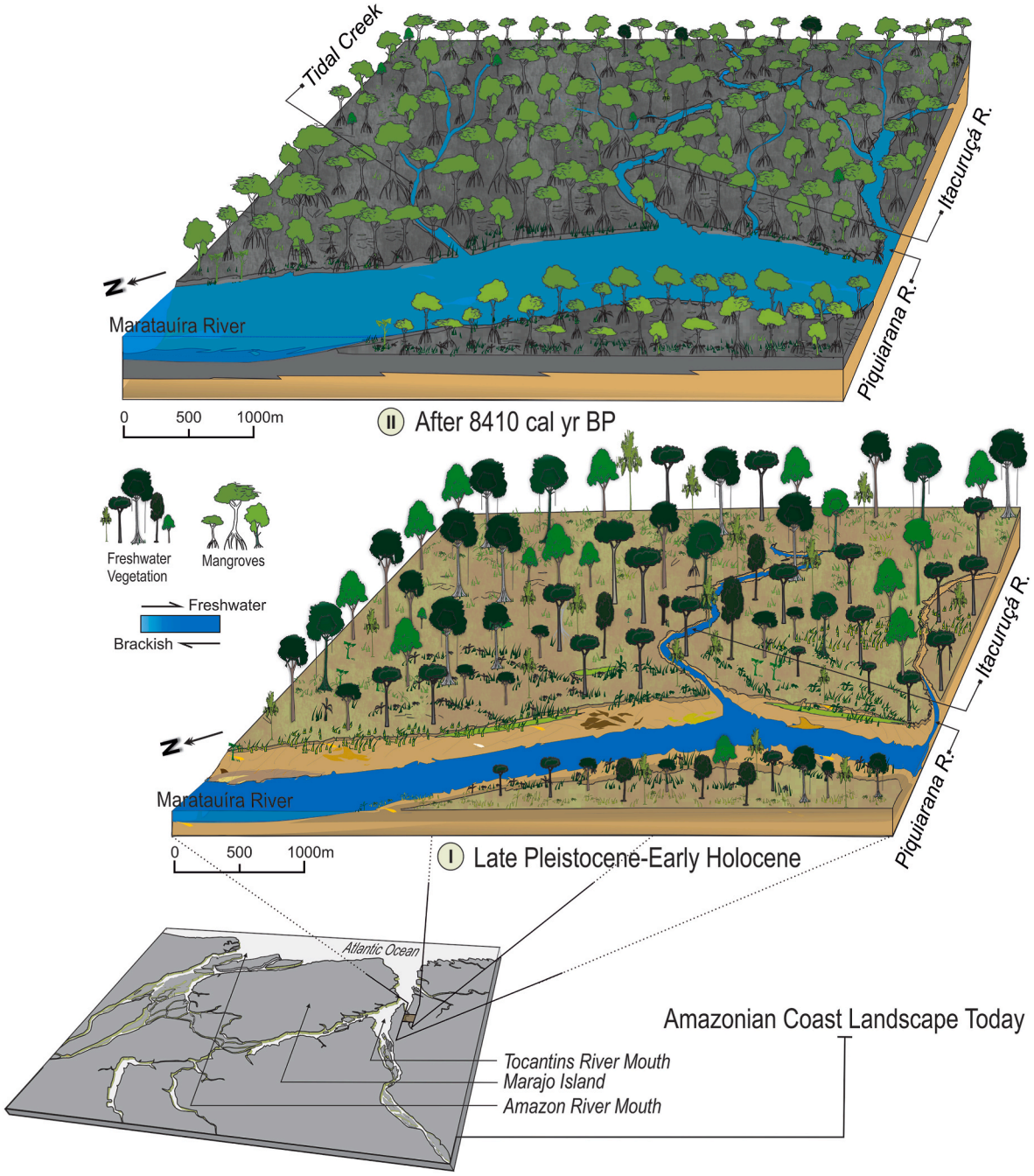

Fig. 4. Conceptual evolution of the landscape from the Itacuruçá plain, at the Amazonian supralittoral, between the early and middle Holocene. The first significant change occurred during post-glacial sea-level rise. The emergence of brackish conditions in a previously fluvial environment (Phase I) led to the establishment of the mangrove swamp, which began to dominate the estuarine landscape since ~8.4 ka yr BP (Phase II).

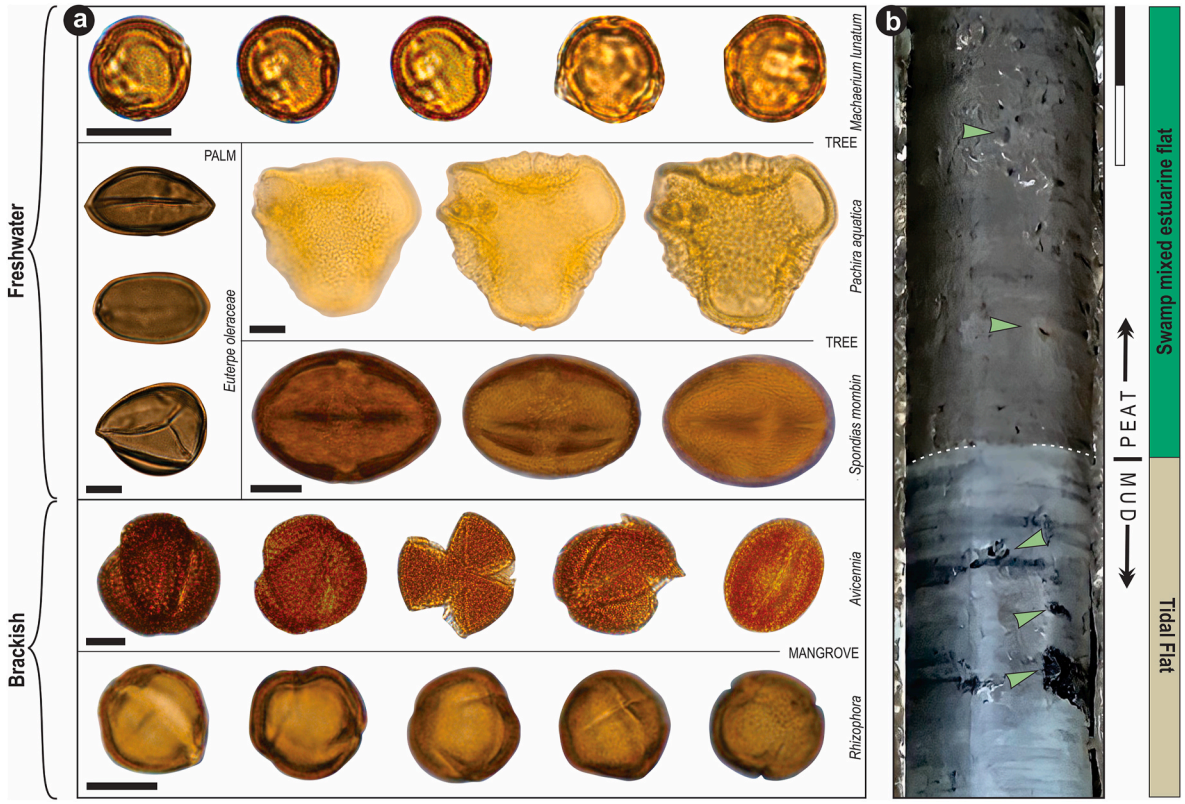

Fig. 5. Photomicrographs of the most representative pollen grains from the mid-late Holocene of the Itacuruçá tidal flat, Amazonian supralittoral, Brazil. The pollen plate is organized as the environmental evolution from the mangroves (brackish) upward to "*várzea*" (freshwater vegetation) (a). The ecological change signature preserved in the sedimentary record (b) indicates abrupt contact between the lower muddy deposit and the uppermost peat deposit. Note overlapping peat conformity to the muddy succession (dashed white line). Bioturbation attributed to woody root as well as dwelling structures produced by the benthic organisms has been pointed with arrows (light green). Pollen scale bar: 10 μm. Core scale bar: 4 cm

fine-grained sands (Dalrymple et al., 2012; Reineck and Wunderlich, 1968). This vertical pattern of facies on the base of the core suggests an estuarine environmental setting established 8410 cal yr BP when the sea level had already reached this sector (Facies Association A). Although this succession coincides with the intertidal zone, recent studies have shown that its position resulted from Late Holocene tectonic activity.

According to Ribeiro (2022), oblique transcurrent structures that control the regional geomorphology led to successive subsidence pulses that affected the sedimentary stacking configuration (Fig. 1c and d). Consequently, the vertical displacement of this succession, which reached >2.1 m compared to the those of upward analogs positioned inland on the mainland, is consistent with subsidence. The overlapping peat-layer offset is a reliable indicator of the downward movement of the muddy deposits. Thus, it is reasonable to postulate that the muddy mangrove deposits (Figs. 2 and 3) formed at least 2 m above this position, an equivalent level to the top of the contemporary supratidal zone, and hence were out of tidal influence (Fig. 1d).

Isotopic data are consistent with the ecological conditions developed in an estuarine setting, with paleoproductivity influenced by terrestrial plants (Fig. 6). For example, the $\delta^{13}C$ value indicates productivity associated with the arrival of C3-plants within the watershed (Meyers, 1994; Qiu et al., 1993), such as mangrove. The binary $\delta^{13}C$ (≥ -25.5) and C/N (≥ 12) suggest OM enrichment by this plant group (Cloern et al., 2002; Meyers, 1997). In addition, the low $\delta^{15}N$ value reinforces the OM of terrestrial plants influencing the Zone 1 infill (Lamb et al., 2006; Meyers, 1994) (Figs. 3 and 6).

As *Rhizophora* grew and colonized the intertidal flats, their complex roots generated strong turbulence, resulting in more sediment traps to expand mudflats horizontally (Bird, 1971; Friess et al., 2012). Mangrove development reshaped the ecological landscape from the dominant

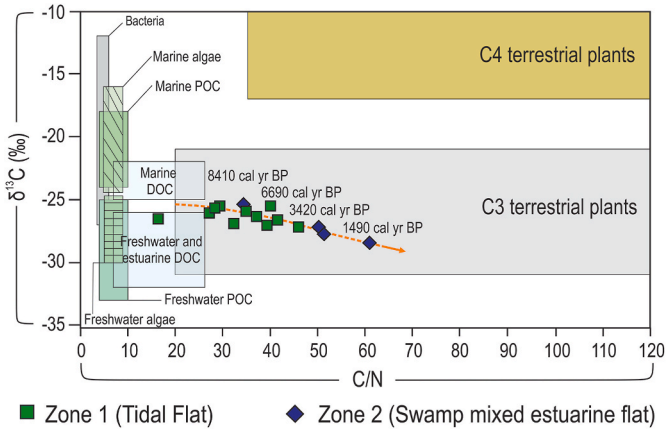

Fig. 6. Binary diagram of $\delta^{13}C$ and C/N for the different facies associations of Tidal flat and Swamp mixed estuarine flat, with interpretation according to data presented by Lamb et al. (2006) Meyers (1997, 1994), Thornton and McManus (1994). The trendline (orange arrow) indicates the increasing paleoproductivity enriched by terrestrial organic matter from the C3 plants from the Zone 1 to Zone 2.

fluvial-ecosystem inherited from the Late Pleistocene (Fig. 4–I) to the brackish forest (Fig. 4–II). Thus, this RSL rise has played a crucial role in the dynamics of the Late Quaternary on the Amazonian coast. Despite its poorly understood effects on inner sub-estuarine systems in the supralittoral region due to the lack of sufficient data to create a model, it can be speculated that the RSL was at least 1.2 ± 0.3 m higher than the current level.

The emerging change from brackish estuary to estuary with the greatest fluvial control on chemistry parameters, that is, the freshwater environment, occurred near the late Holocene (Fig. 7–III). The pollen spectra showed an increase in both trees, *Pachira aquatica* and *Machaerium lunatum*, and freshwater palms, represented mainly by *Euterpe oleracea* and *Mauritia flexuosa* species. Simultaneously, the mangrove began to decrease at 57 cm in the MLT2 core (Figs. 3 and 5a). From 30 cm upward (Zone 2), the pollen percentages suggested both the decline of mangroves and expansion of forests typical of freshwater conditions (Fig. 3).

The RSL likely started to fall, and the saline gradient decreased at approximately ~2000 cal yr BP because freshwater vegetation raised its pollen frequency from the various associations of taxa. This vegetation, which had refugia in the upstream sector since the middle Holocene, began the migration process downstream, growing on former tidal flats previously occupied by mangroves. The freshwater ecosystems became prevalent after 1490 cal yr BP (Fig. 7–IV). Coupled with pollen, the sedimentary system also provides reliable records of this pronounced environmental change and suggests an RSL fall.

The abrupt contact between the lower mangrove (Zone 1) and peat deposits (Zone 2) on the uppermost portion of MLT2 without erosion provides evidence of paleoenvironmental transition (Fig. 5b), indicating that the depositional system did not undergo significant physical changes, such as subaerial exposition. This interpretation is supported by other previously drilled cores (Supplementary F1), which clearly show the contact relation between these two units. Although the age is lacking for these, the analysis of the components, such as the geographical occurrence, thickness, and co-depth, suggests that these peatlands correspond to the same unit, which allows for their correlation. The abrupt basal transition, linked to a lack of erosive contact, indicates that the RSL decline did not force geomorphologic confinement, but instead induced maintenance under tidal inundation frequency (*várzea*), resulting in the present estuarine hydrodynamics.

The organic debris deposition and peat formation along Zone 1 is consistent with both mangrove decline and inundation frequency because peat demands saturated conditions, such as low oxygen contents, to inhibit decomposition, in-depth burial, and preservation in the stratigraphic record (Facies Association B) (Long et al., 2006; Shennan et al., 1996). Presumably, peat is autochthonous and directly related to the paleo-mangrove demise (Fig. 2). The organic-terrestrial character of the C3 plants is supported by geochemistry data, whose $\delta^{13}C$ values presented a mean of −26.4‰ (Meyers, 1997).

The $\delta^{15}N$ average value of 1.8‰ is related to land vascular plants and C/N values increasing from 30 to 62 are also consistent with terrestrial plants as primary organic sources (Meyers, 1997; Thornton and McManus, 1994) (Figs. 2 and 6). The spectral behavior between foraminifera and ferns in the pollen diagrams also helps demonstrate the ecological evolution from brackish to freshwater environments. The fern frequency increased upward in Zone 2, whereas foraminifera decreased (Fig. 3). The behavior of the ferns suggests a mostly freshwater influence (ferns typically occupy streams or lowland regions near the continental swamp) (Berreda et al., 2009), and the foraminifera can be assigned to the diminished brackish water effect, as they are predominantly shallow marine organisms (Long et al., 2006).

5.2. *Mangroves on Itacuruçá tidal flat: new signals regarding the sea-level rise in the Amazon*

Palynological studies on littoral areas worldwide have been critical for assessing paleoecological setting relations at the land-sea interface in tropical and subtropical regions. Many of these have demonstrated that mangrove dynamics are driven by sea-level fluctuations (Ellison, 2005; Engelhart et al., 2007; Hait and Behling, 2009; Punwong et al., 2018; Sloss et al., 2007; Tossou et al., 2008; Woodroffe and Grindrod, 1991). Previous studies on the Amazonian littoral zone reported that the RSL reached its current position near 7000 cal yr BP (Behling and da Costa, 2000; Cohen et al., 2005), with no significant change during the Holocene (Behling et al., 2001; Cohen et al., 2005; Rossetti et al., 2008; Vedel et al., 2006). The mangrove establishment in Itacuruçá is consistent with sea-level rise affecting the supralittoral zone. The age obtained from the MLT core base of approximately 7.6 ka BP was similar to that observed in previous studies (Table 1). Nevertheless, the decline of this mangrove is not consistent with the environmental conditions indicated for the last 8.4 ka BP years of a relatively steady RSL (Fig. 8A).

Mangroves are resilient and tolerate environmental stress, which means that they can survive even high-magnitude changes. In addition to climate change, mangroves are inhibited by nutrient-poor (sandy) soil or higher freshwater inflow (Alongi, 2009). The reduction of muddy sediment input may have a more significant impact if the mangroves span areas subject to sea-level rise (Furukawa and Wolanski, 1996). These conditions can cause asphyxiation from the increase in mean tide level because the lack of sediment supply may limit the vertical accretion of the occupied substrate (Bird, 1971). Moreover, a high input of sand to mangrove substrates can lead to stagnancy or demise of the vegetation, which depends on muddy sediments for root fixation, trunk stability, and ecological growth (1996; Toorman et al., 2018).

The analysis of the MLT2 indicated that the input of muddy sediments was steady over time, including upward gradations by organic debris that developed peat. Peatland is an excellent substrate for this vegetation (cf. Mckee et al., 2007), typically formed due to the root system that traps the own organic matter produced (Cameron and Palmer, 1995). Considering these ecological relationships, peat bogs likely did not restrain mangrove maintenance. However, contrary to mangrove expansion in relation to organic debris deposition, Itacuruçá peats coincide with mangrove pollen reduction frequency. Thus, these are probably the "fingerprint" of mangrove demise (Figs. 2, 7–III and IV).

The pollen spectrum of the peat bed revealed botanical types related to new environmental conditions (Figs. 2 and 3). For example, *Euterpe oleracea*, *Mauritia flexuosa*, *Machaerium lunatum*, *Spondias mombin,* and *Pachira aquatica* were the most representative species (Fig. 5a). This set is typical of freshwater ecosystems, described in several environments with hydrological regimes controlled by freshwater availability (Gomes et al., 2017; Hofmann, 2002). This floodplain vegetation began to thrive over the estuarine plain from 1490 cal yr BP onwards, while the mangrove forest contracted (Fig. 7–III and IV).

In the Amazon, mangroves occurred from the western to eastern littoral sector during the middle Holocene and underwent dynamics that involved spatial disruption. Western mangrove communities were established in tidal flats associated with the Amazon River mouth as a direct consequence of marine incursion after 5560–5470 cal yr BP (Guimarães et al., 2012). In the late Holocene, freshwater input caused the mangrove area to shrink (Cohen et al., 2012). In the central sector of Marajó Island, ~140 km downstream from the study area, a more substantial marine influence caused the mangroves to occupy the intertidal zone between 7328–7168 and 2306–2234 cal yr BP. Subsequently, the mangrove was replaced by freshwater herbs due to increased fluvial discharge (Smith et al., 2011). The eastward mangrove communities at Bragança, in turn, underwent reduction and migration to lowland areas during the mid-Holocene; however, the authors suggest an accentuated RSL decline as the main driving force (Cohen et al., 2021; Vedel et al., 2006).

Except for the eastward mangrove, the dynamics of these wetlands have been assigned to Holocene climate changes. The wet phase and high rainfall conditions increased the Amazon River discharge after 4.2 ka BP, influencing the zone occupied by halophyte vegetation, reducing the saline gradient within the context of sea-level stability, and providing conditions for freshwater forest vegetation (*várzea*) to replace the mangrove (Cohen et al., 2012). Despite this pattern, the estuarine flat from Itacuruçá provides some indicators suggesting that the brackish-to-fluvial environmental shift could have been driven by a natural/forced "cut" of the most high-magnitude mechanism, that is, the

decline in the RSL.

The data still do not indicate that the RSL suffered small oscillations during the middle Holocene after exceeding the current level (Fig. 8A). Nonetheless, based on pollen frequency, geochemistry, and ages, it is possible to infer that the RSL was sufficiently higher than the present level from the middle to late Holocene, providing conditions for this paleo-mangrove to thrive for more than 6.5 ka. Furthermore, the RSL as an outward control for the ecological landscape would be indicated by its "mirrored" characteristic: it influenced mangrove development while restraining the growth of freshwater vegetation (Fig. 3).

Without competition, mangroves prosper in Itacuruçá because of favorable environmental variants, such as seawater influence, and the protection from high-frequency erosive processes such as storms, waves, and tidal currents. Based on the results, it can be concluded that Itacuruçá offers an enhanced opportunity for determining the paleo-sea level rise on the Amazonian inner coast, and this knowledge can help in understanding the flooded embayment setting on the south side of the island of Marajó that was previously attributed to tectonic causes (cf. Barbosa et al., 1974). The RSL decline would also help reinforce the mangrove dynamics/contraction during the late Holocene along north-northwest littoral Amazonian, which is assigned mainly to climate change and freshwater outflow, causing an environmental imbalance in these wetlands.

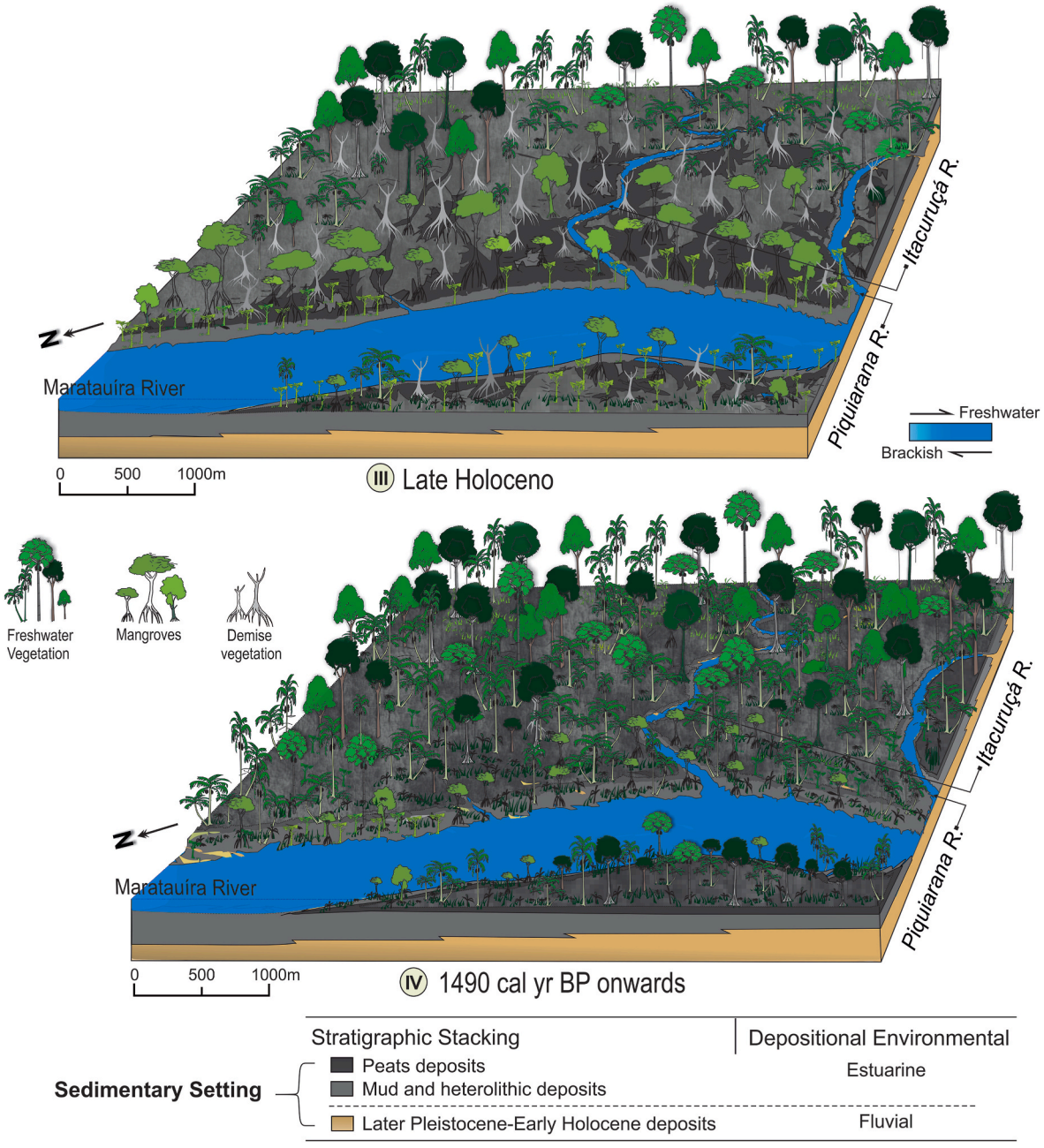

Fig. 7. The mangrove community endured significant spatial loss, while freshwater ecosystems, represented mainly by trees and palms, occupied these areas during the late Holocene (Phase III). In the last phase, freshwater forests nearly completely replaced the mangroves. This environmental change likely resulted from the RSL decline and its stabilization at the current position, which reduced the saline influence and favored the freshwater vegetation domain along the Itacuruçá flat (Phase IV).

5.3. Mangrove dynamic trends in the context of climate change and RSL

Pollen data shows a mangrove occurrence at the supralittoral from ~8410 to 1490 cal yr BP. Since then, the halophyte community nearly disappeared, and was replaced by the freshwater forest in the late Holocene (Figs. 2, 4 and 7). The understanding of the mechanisms behind the mangrove *versus* freshwater vegetation dynamics in the region has indicated precipitation regime changes driven by climate change as an important force. Considering that mangroves develop over mudflats along large river mouths that are sensitive to fluvial discharge variations, the role of climate change cannot be disregarded. Assessment is required to isolate the climatic influence from the non-climatic factors controlling mangroves.

Drier climate trends mark the advance of the saline influence into estuaries due to less fluvial discharge (cf. Potter et al., 2010), which favors the mangrove migration to mudflats landward. This scenario would help understand the Itacuruçá mangroves; however, a drier climate is not consistent with the recent paleoclimatic history of the Amazon. For example, in the Carajás region, upstream of the study area, the pollen spectrum was evaluated by Absy et al. (1991), who gauged the impact of drier conditions in the early and mid-Holocene on the expansion of the open savannah. However, this savannah gave way to a forest complex due to increasing precipitation after 4.4 ka BP. Subsequently, based on geochemical organic and petrographic analyses of sediments from lakes in the same region, Sifeddine et al. (2001) identified that the hydrological regime prevailed from approximately 4.5 ka BP, indicating wetter conditions associated with the development of tropical rainforests (Fig. 8B).

Recently, Guimarães et al. (2021) recognized evidence of a wet climate in this region, in which shallow lakes developed into swamps with herbs and shrubs. Subsequently, at approximately 3 ka BP, the vegetation of the plateaus acquired a structure that marked the establishment of wetter environmental conditions after the drier phase. In general, studies have demonstrated wet climate establishment from the Serra Sul dos Carajás (cf. Absy et al., 1991; Guimarães et al., 2012; Reis et al., 2017; Sifeddine et al., 2001) and other sectors across the continental Amazon (cf. Behling and da Costa, 2000; da Silva et al., 2020; Pessenda et al., 2004, 2001, 1997) to its coastal region (Guimarães et al., 2012; Toledo and Bush, 2008), which have formed a "wetter arch" around this study area since the early-late Holocene (Fig. 8B).

These studies provide a synthesis of past climates on a regional scale and compose a reliable body of evidence that indicates that a wet climate, with a higher rainfall regime similar to current conditions, was present in the region, sharing space and time with mangrove expansion. Thus, the beginning of these climates followed by increased discharge, which is suggested as the trigger to replace mangroves with freshwater vegetation in the Amazon River mouth during the early mid-Holocene, does not explain the paleo-mangrove decline in the Itacuruçá tidal flat. In the Itacuruçá mudflats, the mangroves thrived until the Late Holocene, even under the direct influence of the Tocantins River, with higher freshwater inflow caused by increased rainfall.

The palynological approach provides high-resolution local detection of changes in vegetation (Ellison, 2005) either by external (e.g., Decker et al., 2021) or internal forces (e.g., Ribeiro et al., 2018). If opposing climatic phases affected those wetlands, with freshwater advancing over the halophyte environment, its record should have been well preserved in the pollen, with an increased frequency of the freshwater genera, rather than mangroves. However, the present study did not recognize these signals imprinted at the MLT2 core through pollen content, and thus isolated climate noise. In contrast, the pollen representativeness from the mangrove indicate their forest dominance in this estuary. Thus, the hypothetical scenario of a long-lasting dry climate is inconsistent with the data presented here as well as those of other studies performed along the wetter arch (Fig. 8B). The eventual wet conditions were not sufficient to affect the paleo-mangrove, probably because the magnitude of the brackish influence caused by the RSL rise exceeded the site of occupation.

These findings link the paleo-mangrove and its dynamics to a trending RSL change. The RSL highstand since 8410 cal yr BP probably helped develop and expand the paleo-mangroves. In contrast, its decline over the last two millennia represents the main force behind its reduction and area loss, and the subsequent appearance of freshwater vegetation on tidal flats at approximately 1490 cal yr BP (Fig. 8A). We are not suggesting that there was no high input or increase in the drainage network's fluvial discharge due to wetter climates. Based on the analysis of our data, we argue that the influence of increased freshwater discharge, which could impact mangrove dynamics, may have been weakened by a more intense marine effect from the mid-late Holocene in this estuary.

The RSL highstand signals from the supralittoral allow for reevaluation of the marine incursion in the region, in this case, characterized by a probable rapid rise during the middle Holocene, followed by stabilization and an equally rapid fall in the late Holocene (Fig. 8A). Such data will help to gather evidence to improve the curve model for the north Brazilian coast in different time-space scales. Similarly, considering the paleo-incursion peak at 1.2 ± 0.3 above the present-day level, the curve

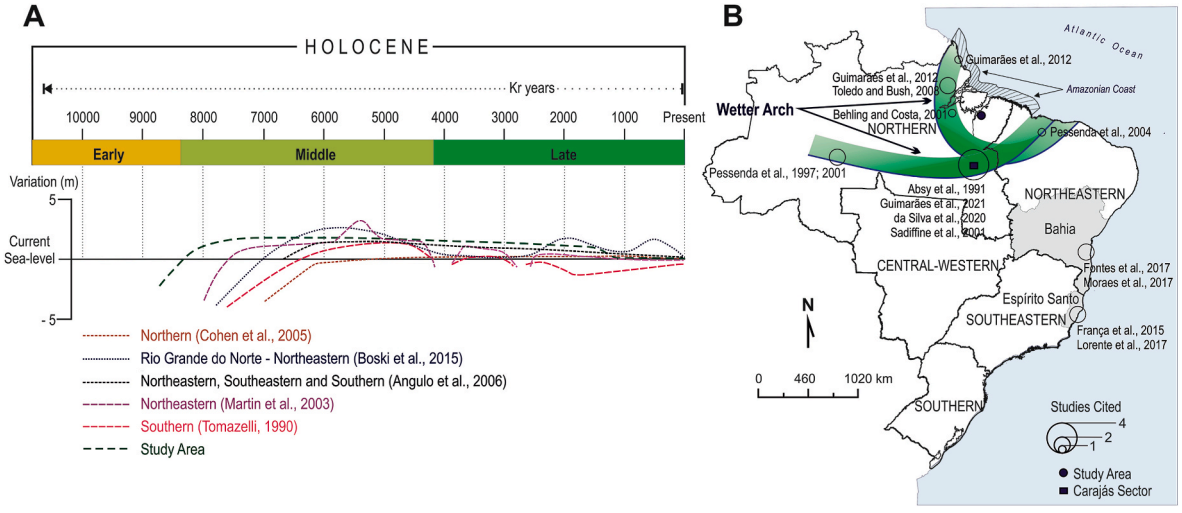

Fig. 8. Summary of sea-level rise curves for Brazilian regions during the Holocene (A). The sea level curve proposed for the study area is plotted in the diagram. According to several studies, wet climates were present in several sectors of the Amazon region during the Late Holocene. These sectors comprise a wetter climate arch upstream of the study area (B).

of the RSL for the Amazonian coast would probably become more analogous to that of the northeastern and south-southeastern Brazil littoral zones, reflecting a general trend instead of the contrast previously suggested (Fig. 8A). Several authors agree that the sea-level rise attained a peak 2–5 m above the present level over the Holocene, before decreasing during the late Holocene to the present level (Angulo et al., 2006; Bezerra et al., 2003; Boski et al., 2015; Castro et al., 2014; Martin et al., 2003; Suguio et al., 2013; Tomazelli, 1990). The mangroves nearly disappeared as they migrated seaward during the Late Holocene in the Espírito Santo littoral zone in the southeastern region (França et al., 2015) and at Bahia on the northeastern coast in response to relative sea-level decline (Fontes et al., 2017; Moraes et al., 2017) (Fig. 8A).

6. Conclusions

This study evaluated the pollen content of a sediment core retrieved from the Itacuruçá flat in the Amazonian supralittoral region. Pollen data integrated with sedimentary features, chronological ages, and elementary data ($\delta^{13}C$, $\delta^{15}N$, and C/N) showed that the marine influence in this sector was more intense than that presently. A mangrove community occupied the muddy flats 180 km from the shoreline for over 6 ka BP, between 8410 and 1490 cal yr BP. It is likely that this halophyte community was established because of post-glacial sea-level rise, which exceeded the current level. After 1490 cal yr BP, the landscape witnessed mangrove contraction, and freshwater vegetation became the dominant forest. Organic debris deposition in the sedimentary record was consistent with mangrove decline, and such environmental changes may be related to the RSL decline instead of the influence of climate change.

Our results suggest that the RSL rapidly increased during the middle Holocene, followed by stabilization and an equally rapid decrease to its present-day position near the two last millennia; this finding is inconsistent with previous investigations addressing the Amazonian coast. Accordingly, advances are necessary to understand the causes and trends of RSL variables in the late Holocene and gather evidence to improve the RSL curve model for the north Brazilian coast. Here, the paleo-mangrove is the leading benchmark of marine incursion, primarily because of its establishment in a field far from the coastline. These distant fields provide reliable archives for understanding RSL oscillations, allowing for the unraveling of ecological dynamics and, consequently, the development of the most robust paleogeographic models.

CRediT authorship contribution statement

Samuel Rodrigues Ribeiro: Writing – review & editing, Writing – original draft, Visualization, Validation, Supervision, Software, Resources, Project administration, Methodology, Investigation, Formal analysis, Data curation, Conceptualization. **Roberto Célio Valadão:** Visualization, Supervision, Formal analysis, Data curation, Resources, Writing - review & editing. **Makênia Oliveira Soares Gomes:** Visualization, Validation, Formal analysis, Data curation, Resources. **Jonathas S. Bittencourt:** Visualization, Validation, Formal analysis, Data curation, Writing - review & editing. **Raquel Araújo Alves:** Visualization, Formal analysis, Data curation, Validation.

Declaration of competing interest

The authors declare that they have no known competing financial interests or personal relationships that could have appeared to influence the work reported in this paper.

Data availability

The authors are unable or have chosen not to specify which data has been used.

Acknowledgments

The authors thank the members of the Laboratory of Paleontology and Macroevolution (CPMTC-UFMG) and the Graduate Program of Geography support (IGC-UFMG). Appreciation is expressed to Mr. Raimundo R, João M., Joárison and Jessé M., and Roberto A. for their assistance throughout the fieldwork. We thank Fernando César for his support through the Geomorphology Laboratory (UFMG). The first author thanks CAPES for the doctoral scholarship (Finance Code 001). JS Bittencourt would like thanks to FAPEMIG (grant PPM-00304-18) for financial support and CNPq (productivity fellowship). We are grateful to the anonymous reviewers for their valuable comments and suggestions.

Appendix A. Supplementary data

Supplementary data to this article can be found online at https://doi.org/10.1016/j.jsames.2023.104422.

References

Absy, M.L., Cleef, A., Fournier, M., Martin, L., Servant, M., Sifeddine, A., Silva, M.F. da, Soubies, F., Suguio, K., Turcq, B., van der Hammen, T., 1991. Mise en évidence de quatre phases d'ouverture de la forêt dense dans le sud-est de l'Amazonie au cours des 60000 dernières années: première comparaison avec d'autres régions tropicales. Comptes Rendus de L"Academie des Sciences, Série II, 312, 673-678.

Absy, M.L., 1975. Polen e esporos do Quaternário de Santos (Brasil). HOEHNEA 5, 1–26.

Allen, G.P., Posamentier, H.W., 1993. Sequence stratigraphy and facies model of an incised valley fill; the Gironde Estuary, France. J. Sediment. Res. 63, 378–391. https://doi.org/10.1306/D4267B09-2B26-11D7-8648000102C1865D.

Alongi, D.M., 2009. The Energetics of Mangrove Forests. The Energetics of Mangrove Forests 1–216. https://doi.org/10.1007/978-1-4020-4271-3.

ANA (national waters agency). November 2019. Available. http://www.snirh.gov.br/hidrotelemetria.

Angulo, R.J., Lessa, G.C., 1997. The Brazilian sea-level curves: a critical review with emphasis on the curves from the Paranaguá and Cananéia regions. Mar. Geol. 140, 141–166. https://doi.org/10.1016/S0025-3227(97)00015-7.

Angulo, R.J., Lessa, G.C., Souza, M.C. de, 2006. A critical review of mid- to late-Holocene sea-level fluctuations on the eastern Brazilian coastline. Quat. Sci. Rev. 25, 486–506. https://doi.org/10.1016/j.quascirev.2005.03.008.

Aziz, I., Khan, M.A.M., 2001. Effect of seawater on the growth, ion content and water potential of Rhizophora mucronata lam. J. Plant Res. 114, 369–373. https://doi.org/10.1007/PL00013998.

Ball, M., 1998. Mangrove species richness in relation to salinity and waterlogging: a case study along the Adelaide River floodplain, northern Australia. Global Ecol. Biogeogr. Lett. 7, 73–82. https://doi.org/10.1111/J.1466-8238.1998.00282.X.

Barbosa, G.V., Rennó, C.V., Franco, E.M.S., 1974. Geomorfologia da Folha SA-22 Belém. In: DNPM (Ed.), Folha SA.22 Belém: geologia, geomorfologia, solos, vegetação, uso potential da terra, pp. 70–130. Rio de Janeiro.

Behling, H., Cohen, M.C.L., Lara, R.J., 2001. Studies on holocene mangrove ecosystem dynamics of the Bragança peninsula in north-eastern Pará, Brazil. Palaeogeogr. Palaeoclimatol. Palaeoecol. 167, 225–242. https://doi.org/10.1016/S0031-0182(00)00239-X.

Behling, H., da Costa, M.L., 2000. Holocene environmental changes from the rio curua record in the caxiuana region, eastern Amazon basin. Quat. Res. 53, 369–377. https://doi.org/10.1006/qres.1999.2117.

Berreda, V., Palazzesi, L., Marenssi, S., 2009. Palynological record of the paleogene río leona formation (southernmost south America): stratigraphical and paleoenvironmental implications. Rev. Palaeobot. Palynol. 154, 22–33. https://doi.org/10.1016/j.revpalbo.2008.11.005.

Bezerra, F.H.R., Barreto, A.M.F., Suguio, K., 2003. Holocene sea-Level history on the rio Grande do norte state coast, Brazil. Mar. Geol. 196, 73–89. https://doi.org/10.1016/S0025-3227(03)00044-6.

Bird, E.C.F., 1971. Mangroves as land-builders. Victorian Nat. 88, 189–197.

Blasco, F., Saenger, P., Janodet, E., 1996. Mangroves as indicators of coastal change. Catena 27, 167–178. https://doi.org/10.1016/0341-8162(96)00013-6.

Boski, T., Bezerra, F.H.R., de Fátima Pereira, L., Souza, A.M., Maia, R.P., Lima-Filho, F.P., 2015. Sea-level rise since 8.2ka recorded in the sediments of the potengi-jundiai estuary, NE brasil. Mar. Geol. 365, 1–13. https://doi.org/10.1016/j.margeo.2015.04.003.

Cameron, C.C., Palmer, C.A., 1995. The Mangrove Peat of the Tobacco Range Islands. Belize Barrier Reef, Central America.

Castro, J.W.A., Suguio, K., Seoane, J.C.S., da Cunha, A.M., Dias, F.F., 2014. Sea-level fluctuations and coastal evolution in the state of Rio de Janeiro, southeastern Brazil. An Acad. Bras Ciências 86, 671–683. https://doi.org/10.1590/0001-3765201420140007.

Cloern, J.E., Canuel, E.A., Harris, D., 2002. Stable carbon and nitrogen isotope composition of aquatic and terrestrial plants of the San Francisco Bay estuarine system. Limnol. Oceanogr. 47, 713–729. https://doi.org/10.4319/LO.2002.47.3.0713.

Cohen, M.C.L., Behling, H., Lara, R.J., 2005. Amazonian mangrove dynamics during the last millennium: the relative sea-level and the Little Ice Age. Rev. Palaeobot. Palynol. 136, 93–108. https://doi.org/10.1016/j.revpalbo.2005.05.002.

Cohen, M.C.L., Camargo, P.M.P., Pessenda, L.C.R., Lorente, F.L., de Souza, A.v., Corrêa, J.A.M., Bendassolli, J., Dietz, M., 2021. Effects of the middle Holocene high sea-level stand and climate on Amazonian mangroves. J. Quat. Sci. 36, 1013–1027. https://doi.org/10.1002/jqs.3343.

Cohen, M.C.L., Pessenda, L.C.R., Behling, H., de Fátima Rossetti, D., França, M.C., Guimarães, J.T.F., Friaes, Y., Smith, C.B., 2012. Holocene palaeoenvironmental history of the Amazonian mangrove belt. Quat. Sci. Rev. 55, 50–58. https://doi.org/10.1016/j.quascirev.2012.08.019.

Colinvaux, P., De Oliveira, P.E., Patiño, J.E.M., 1999. Amazon Pollen Manual and Atlas. Harwood Academic Publishers, Dordrecht.

da Silva, E.F., Lopes, K. da S., Alves, R., Carreira, L.M.M., Silva, D.F. da, Romeiro, L. de A., Batista Júnior, W.F., Rodrigues, T.M., Secco, R. de S., Guimarães, J.T.F., 2020. Hydroclimate influences on modern pollen rain of upland southeastern Amazonia. Holocene 30, 721–732. https://doi.org/10.1177/0959683619895586.

Daidu, F., Yuan, W., Min, L., 2013. Classifications, sedimentary features and facies associations of tidal flats. J. Palaeogeogr. 2, 66–80. https://doi.org/10.3724/SP.J.1261.2013.00018.

Deines, P., 1980. The isotopic composition of reduced organic carbon. In: Fritz, P., Fontes, J.C. (Eds.), Handbook of Environmental Isotope Geochemistry. The Terrestrial Environment, vol. 1. Elsevier, Amsterdam, pp. 329–406.

Dalrymple, R.W., Boyd, R., Zaitlin, B.A., 1994. Incised-Valley Systems: Origin and Sedimentary Sequences. Incised-Valley Systems<subtitle>Origin and Sedimentary Sequences</subtitle>. https://doi.org/10.2110/PEC.94.12.

Dalrymple, R.W., Choi, K., 2007. Morphologic and facies trends through the fluvial-marine transition in tide-dominated depositional systems: a schematic framework for environmental and sequence-stratigraphic interpretation. Earth Sci. Rev. 81, 135–174. https://doi.org/10.1016/j.earscirev.2006.10.002.

Dalrymple, R.W., Mackay, D.A., Ichaso, A.A., Choi, K.S., 2012. Processes, morphodynamics, and facies of tide-dominated estuaries. Principles of Tidal Sedimentology 79–107. https://doi.org/10.1007/978-94-007-0123-6_5.

Dayan, H., le Cozannet, G., Speich, S., Thiéblemont, R., 2021. High-end scenarios of Sea-Level rise for coastal risk-averse stakeholders. Front. Mar. Sci. 8, 514. https://doi.org/10.3389/fmars.2021.569992/bibtex.

Decker, V., Falkenroth, M., Lindauer, S., Landgraf, J., Al-Lawati, Z., Al-Rahbi, H., Franz, S.O., Hoffmann, G., 2021. Collapse of Holocene mangrove ecosystems along the coastline of Oman. Quat. Res. 100, 52–76. https://doi.org/10.1017/qua.2020.96.

Dominguez, J.M.L., Bittencourt, A.C.S.P., Leão, Z.M.A.N., Azevedo, A.E.G., 1990. Geologia do Quaternário costeiro do estado de Pernambuco. Rev. Bras. Geociencias 20, 208–215.

Ellison, J., 2005. Holocene palynology and sea-level change in two estuaries in Southern Irian Jaya. Palaeogeogr. Palaeoclimatol. Palaeoecol. 220, 291–309. https://doi.org/10.1016/J.palaeo.2005.01.008.

Engelhart, S.E., Horton, B.P., Roberts, D.H., Bryant, C.L., Corbett, D.R., 2007. Mangrove pollen of Indonesia and its suitability as a sea-level indicator. Mar. Geol. 242, 65–81. https://doi.org/10.1016/J.margeo.2007.02.020.

Erdtman, G., 1960. The acetolysis method: in a revised description. Svensk Botanisk Tidskrift Lund 54, 561–564.

Evans, G., Prego, R., 2003. Rias, estuaries and incised valleys: is a ria an estuary? Mar. Geol. 196, 171–175. https://doi.org/10.1016/S0025-3227(03)00048-3.

Fapespa, 2016. Amazon Foundation for Studies and Research Support. Pará Municipal Statistics: Igarapé-Miri. Belém. June 2019. Available: https://www.fapespa.pa.gov.br/node/201.

Ferreira, C.S., 1977. Fácies da Formação Pirabas (Mioceno Inferior): novos conceitos e ampliações. Natl. Acad. Brás. Ciênc. 49, 353.

Fontes, N.A., Moraes, C.A., Cohen, M.C.L., Alves, I.C.C., França, M.C., Pessenda, L.C.R., Francisquini, M.I., Bendassolli, J.A., Macario, K., Mayle, F., 2017. The impacts of the middle holocene high Sea-Level stand and climatic changes on mangroves of the jucuruçu river, southern Bahia-Northeastern Brazil. Radiocarbon 59, 215–230. https://doi.org/10.1017/rdc.2017.6.

França, M.C., Alves, I.C.C., Castro, D.F., Cohen, M.C.L., Rossetti, D.F., Pessenda, L.C.R., Lorente, F.L., Fontes, N.A., Junior, A.Á.B., Giannini, P.C.F., Francisquini, M.I., 2015. A multi-proxy evidence for the transition from estuarine mangroves to deltaic freshwater marshes, Southeastern Brazil, due to climatic and sea-level changes during the late Holocene. Catena 128, 155–166. https://doi.org/10.1016/J.catena.2015.02.005.

Friess, D.A., Krauss, K.W., Horstman, E.M., Balke, T., Bouma, T.J., Galli, D., Webb, E.L., 2012. Are all intertidal wetlands naturally created equal? Bottlenecks, thresholds and knowledge gaps to mangrove and saltmarsh ecosystems. Biol. Rev. 87, 346–366. https://doi.org/10.1111/J.1469-185X.2011.00198.X.

Furukawa, K., Wolanski, E., 1996. Sedimentation in mangrove forests. Mangroves Salt Marshes 1 1, 3–10. https://doi.org/10.1023/A:1025973426404, 1996 1.

Galili, E., Zviely, D., Weinstein-Evron, M., 2005. Holocene sea-level changes and landscape evolution on the northern Carmel coast (Israel). Méditerranée 79–86. https://doi.org/10.4000/mediterranee.1912.

Ghandour, I.M., Al-Zubieri, A.G., Basaham, A.S., Mannaa, A.A., Al-Dubai, T.A., Jones, B.G., 2021. Mid-late holocene paleoenvironmental and sea level reconstruction on the Al lith red sea coast, Saudi arabia. Front. Mar. Sci. 744. https://doi.org/10.3389/FMARS.2021.677010, 0.

Gilman, E.L., Ellison, J., Duke, N.C., Field, C., 2008. Threats to mangroves from climate change and adaptation options: a review. Aquat. Bot. https://doi.org/10.1016/j.aquabot.2007.12.009.

Góes, A.M., Rossetti, D. de F., Nogueira, A.C.R., Toledo, P.M. de, 1990. Modelo Deposicional preliminar da Formação Pirabas no Nordeste do Estado do Pará. Boletim do Museu Paraense Emílio Goeldi. Cien. Terra 2, 3–15.

Gomes, M.O.S., Meyer, K.E.B., Pessenda, L.C.R., 2017. Reconstituição paleoambiental da Vereda Carrasco da Raposa, Parque Estadual da Serra do Cabral, MG, Brasil, por meio de estudos palinológico e isotópico. Pesqui. em Geociencias 44, 41–62. https://doi.org/10.22456/1807-9806.79586.

Grimm, E.C., 1987. CONISS: a FORTRAN 77 program for stratigraphically constrained cluster analysis by the method of incremental sum of squares. Comput. Geosci. 13, 13–35. https://doi.org/10.1016/0098-3004(87)90022-7.

Guimarães, J.T.F., Cohen, M.C.L., Pessenda, L.C.R., França, M.C., Smith, C.B., Nogueira, A.C.R., 2012. Mid- and late-Holocene sedimentary process and palaeovegetation changes near the mouth of the Amazon River. Holocene 22, 359–370. https://doi.org/10.1177/0959683611423693.

Guimarães, J.T.F., Sahoo, P.K., de Figueiredo, M.M.J.C., da Silva Lopes, K., Gastauer, M., Ramos, S.J., Caldeira, C.F., Souza-Filho, P.W.M., Reis, L.S., da Silva, M.S., Pontes, P.R., da Silva, R.O., Rodrigues, T.M., 2021. Lake sedimentary processes and vegetation changes over the last 45k cal a bp in the uplands of south-eastern Amazonia. J. Quat. Sci. 36, 255–272. https://doi.org/10.1002/jqs.3268.

Haines, E.B., 1976. Stable carbon isotope ratios in the biota soils and tidal water of a Georgia USA salt marsh. Estuar. Coast Mar. Sci. 4, 609–616.

Hait, A.K., Behling, H., 2009. Holocene mangrove and coastal environmental changes in the western Ganga-Brahmaputra Delta, India. Veg. Hist. Archaeobotany 18, 159–169. https://doi.org/10.1007/S00334-008-0203-5.

Hofmann, C.C., 2002. Pollen distribution in sub-Recent sedimentary environments of the Orinoco Delta (Venezuela) – an actuo-palaeobotanical study. Rev. Palaeobot. Palynol. 119, 191–217. https://doi.org/10.1016/S0034-6667(01)00141-5.

Hogg, A.G., Heaton, T.J., Hua, Q., Palmer, J.G., Turney, C.S.M., Southon, J., Bayliss, A., Blackwe Boswijk, G., Bronk Ramsey, C., Pearson, C., Petchey, F., Reimer, P., Reimer, R., Wacker, L., 2020. SHCal20 southern hemisphere calibration, 0–55,000 Years cal BP. Radiocarbon 62, 759–778. https://doi.org/10.1017/RDC.2020.59.

Jayatissa, L.P., Wickramasinghe, W.A.A.D.L., Dahdouh-Guebas, F., Huxham, M., 2008. Interspecific variations in responses of mangrove seedlings to two contrasting salinities. Int. Rev. Hydrobiol. 93, 700–710. https://doi.org/10.1002/iroh.200711017.

Kelletat, D.H., 2019. Holocene Coastal Geomorphology 977–980. https://doi.org/10.1007/978-3-319-93806-6_171.

Kodikara, K.A.S., Jayatissa, L.P., Huxham, M., Dahdouh-Guebas, F., Koedam, N., 2018. The effects of salinity on growth and survival of mangrove seedlings changes with age. Acta Bot. Bras. 32, 37–46. https://doi.org/10.1590/0102-33062017ABB0100.

Lamb, A.L., Wilson, G.P., Leng, M.J., 2006. A review of coastal palaeoclimate and relative sea-level reconstructions using δ13C and C/N ratios in organic material. Earth Sci. Rev. 75, 29–57. https://doi.org/10.1016/J.earscirev.2005.10.003.

Long, A.J., Waller, M.P., Stupples, P., 2006. Driving mechanisms of coastal change: peat compaction and the destruction of late Holocene coastal wetlands. Mar. Geol. 225, 63–84. https://doi.org/10.1016/j.margeo.2005.09.004.

Lugo, A.E., Snedaker, S.C., 1974. The ecology of mangroves. Annu. Rev. Ecol. Systemat. 5, 39–64. https://doi.org/10.1146/annurev.ES.05.110174.000351.

Martin, L., Dominguez, J.M.L., Bittencourt, A.C.S.P., 2003. Fluctuating Holocene sea levels is eastern and southeastern Brazil: evidence from a multiple fossil and geometric indicators. J. Coast Res. 19, 101–124.

Mckee, K.L., Cahoon, D.R., Feller, I.C., 2007. Caribbean mangroves adjust to rising sea level through biotic controls on change in soil elevation. Global Ecol. Biogeogr. 16, 545–556. https://doi.org/10.1111/J.1466-8238.2007.00317.X.

Meyers, P.A., 1997. Organic geochemical proxies of paleoceanographic. Org. Geochem. 27, 213–250.

Meyers, P.A., 1994. Preservation of elemental and isotopic source identification of sedimentary organic matter. Chem. Geol. 114, 289–302. https://doi.org/10.1016/0009-2541(94)90059-0.

Miall, 1978. Facies types and vertical profilemodels in braided river deposits: a summary. In: Miall, A.D. (Ed.), Fluvial Sedimentology. Canadian Society of Petroleum, pp. 597–604. Geologists, Calgary.

Moraes, C.A., Fontes, N.A., Cohen, M.C.L., França, M.C., Pessenda, L.C.R., Rossetti, D.F., Francisquini, M.I., Bendassolli, J.A., Macario, K., 2017. Late Holocene mangrove dynamics dominated by autogenic processes. Earth Surf. Process. Landforms 42, 2013–2023. https://doi.org/10.1002/ESP.4167.

Mukherjee, N., Dahdouh-Guebas, F., Koedam, N., Shanker, K., 2015. An interdisciplinary framework to evaluate bioshield plantations: insights from peninsular India. Acta Oecol. 63, 91–100. https://doi.org/10.1016/J.ACTAO.2014.01.005.

Munsell Soil Color Charts, New Revised Edition, 2009. Macbeth Division of Kollmorgen Instruments, New Windsor, NY.

Murray, J.W., Alve, E., 1999. Natural dissolution of modern shallow water benthic foraminifera: taphonomic effects on the palaeoecological record. Palaeogeogr. Palaeoclimatol. Palaeoecol. 146, 195–209. https://doi.org/10.1016/S0031-0182(98)00132-1.

Naidoo, G., 1985. Effects of waterlogging and salinity on plant-water relations and on the accumulation of solutes in three mangrove species. Aquat. Bot. 22, 133–143. https://doi.org/10.1016/0304-3770(85)90042-7.

Panapitukkul, N., Duarte, C.M., Thampanya, U., Kheowvongsri, P., Srichai, N., Geertz-Hansen, O., Terrados, J., Boromthanarath, S., 1998. Mangrove colonization: mangrove progression over the growing pak phanang (SE Thailand) mud flat. Estuar. Coast Shelf Sci. 47, 51–61. https://doi.org/10.1006/ECSS.1998.0343.

Pessenda, L.C.R., Ribeiro, A. de S., Marques Gouveia, S.E., Aravena, R., Boulet, R., Bendassolli, J.A., 2004. Vegetation dynamics during the late Pleistocene in the Barreirinhas region, Maranhão State, northeastern Brazil, based on carbon Isotopes

in soil organic matter. Quat. Res. 62, 183–193. https://doi.org/10.1016/J.yqres.2004.06.003.
Pessenda, L.C.R., Boulet, R., Aravena, R., Rosolen, V., Gouveia, S.E.M., Ribeiro, A.S., Lamotte, M., 2001. Origin and dynamics of soil organic matter and vegetation changes during the Holocene in a forest-savanna transition zone, Brazilian Amazon region. Holocene 11, 250–254. https://doi.org/10.1191/095968301668898509.
Pessenda, L.C.R., Gouveia, S.E.M., Aravena, R., Gomes, B.M., Boulet, R., Ribeiro, A.S., 1997. 14C dating and stable carbon isotopes of soil organic matter in forest–savanna boundary areas in the southern Brazilian Amazon region. Radiocarbon 40, 1013–1022. https://doi.org/10.1017/S0033822200018981.
Polidoro, B.A., Carpenter, K.E., Collins, L., Duke, N.C., Ellison, A.M., Ellison, J.C., Farnsworth, E.J., Fernando, E.S., Kathiresan, K., Koedam, N.E., Livingstone, S.R., Miyagi, T., Moore, G.E., Nam, V.N., Ong, J.E., Primavera, J.H., Salmo, S.G., Sanciangco, J.C., Sukardjo, S., Wang, Y., Yong, J.W.H., 2010. The loss of species: mangrove extinction risk and geographic areas of global concern. PLoS One 5, e10095. https://doi.org/10.1371/journal.pone.0010095.
Potter, I.C., Chuwen, B.M., Hoeksema, S.D., Elliott, M., 2010. The concept of an estuary: a definition that incorporates systems which can become closed to the ocean and hypersaline. Estuar. Coast Shelf Sci. 87, 497–500. https://doi.org/10.1016/J.ECSS.2010.01.021.
Prestes, Y.O., Borba, T.A., da, C., Silva, A.C. da, Rollnic, M., 2020. A discharge stationary model for the Pará-Amazon estuarine system. J. Hydrol.: Reg. Stud. 28 https://doi.org/10.1016/j.ejrh.2020.100668.
Punwong, P., Selby, K., Marchant, R., 2018. Holocene mangrove dynamics and relative sea-level changes along the Tanzanian coast, East Africa. Estuarine. Coastal and Shelf Science 212, 105–117. https://doi.org/10.1016/J.ecss.2018.07.004.
Qiu, L., Williams, D.F., Gvorzdkov, A., Karabanov, E., Shimaraeva, M., 1993. Biogenic silica accumulation and paleoproductivity in the northern basin of Lake Baikal during the Holocene. Geology 21, 25–28. https://doi.org/10.1130/0091-7613(1993)021<0025:BSAAPI>2.3.CO, 2.
Reineck, H.E., Wunderlich, F., 1968. Classification and origin of flaser and lenticular bedding. Sedimentology 11, 99–104. https://doi.org/10.1111/j.1365-3091.1968.tb00843.x.
Reading, H.G., 1996. Sedimentary Environments: Processes, Facies and Stratigraphy, third ed. Blackwell, Oxford, p. 689.
Reis, L.S., Guimarães, J.T.F., Souza-Filho, P.W.M., Sahoo, P.K., de Figueiredo, M.M.J.C., de Souza, E.B., Giannini, T.C., 2017. Environmental and vegetation changes in southeastern Amazonia during the late Pleistocene and Holocene. Quat. Int. 449, 83–105. https://doi.org/10.1016/J.quaint.2017.04.031.
Ribeiro, S.R., 2022. Morfogênese e evolução paleogeográfica da foz do Rio Tocantins, Estado do Pará, durante o Holoceno. PhD thesis, Belo Horizonte. Universidade Federal de Minas Gerais, p. 191.
Ribeiro, S.R., Valadão, R.C., 2021. Efeitos marinho e fluvial na dinâmica dos ambientes inundáveis do Estuário Superior do Rio Pará, Norte do Brasil. Revista Brasileira de Geomorfologia 22, 76–98. https://doi.org/10.20502/rbg.v22i4.2017.
Ribeiro, S.R., Valadão, R.C., 2020. Processos fluviomarinhos associados à formação da Ilha Rasa, Sul da Baía de Marapatá, Nordeste do Pará, Brasil. Arq. Ciencias do Mar 53, 110–119. https://doi.org/10.32360/acmar.v53,supl, 42659.
Ribeiro, S.R., Batista, E.J.L., Cohen, M.C.L., França, M.C., Pessenda, L.C.R., Fontes, N.A., Alves, I.C.C., Bendassolli, J.A., 2018. Allogenic and autogenic effects on mangrove dynamics from the Ceará Mirim River, north-eastern Brazil, during the middle and late Holocene. Earth Surf. Process. Landforms 43, 1622–1635. https://doi.org/10.1002/esp.4342.
Rossetti, D.F., Valeriano, M.M., Góes, A.M., Thales, M., 2008. Palaeodrainage on Marajó Island, northern Brazil, in relation to Holocene relative sea-level dynamics. Holocene 18, 923–934. https://doi.org/10.1177/0959683608091798.
Rossetti, D.F., Truckenbrodt, W., Góes, A.M., 1989. Estudo paleoambiental e estratigráfico dos Sedimentos Barreiras e Pós-Barreiras na região Bragantina, nordeste do Pará. Boletim do Museu Paraense Emílio Goeldi. Série Ciências da Terra 1, 25–74.
Roubik, D.W., Moreno, J.E., 1991. Pollen and Spores of Barro Colorado Island. Missouri Botanical Garden, St Louis.
Sampath, D.M.R., Boski, T., Loureiro, C., Sousa, C., 2015. Modelling of estuarine response to sea-level rise during the holocene: application to the guadiana estuary–SW iberia. Geomorphology 232, 47–64. https://doi.org/10.1016/J.geomorph.2014.12.037.
Shennan, I., Long, A.J., Rutherford, M.M., Green, F.M., Innes, J.B., Lloyd, J.M., Zong, Y., Walker, K.J., 1996. Tidal marsh stratigraphy, sea-level change and large earthquakes, I: A 5000 year record in Washington, U.S.A. Quat. Sci. Rev. 15, 1023–1059. https://doi.org/10.1016/S0277-3791(96)00007-8.
Sifeddine, A., Martin, L., Turcq, B., Volkmer-Ribeiro, C., Soubiès, F., Cordeiro, R.C., Suguio, K., 2001. Variations of the Amazonian rainforest environment: a sedimentological record covering 30,000 years. Palaeogeogr. Palaeoclimatol. Palaeoecol. 168, 221–235. https://doi.org/10.1016/S0031-0182(00)00256-X.
Sloss, C.R., Murray-Wallace, C.V., Jones, B.G., 2007. Holocene sea-level change on the southeast coast of Australia: a review. undefined 17, 999–1014. https://doi.org/10.1177/0959683607082415.
Smith, C.B., Cohen, M.C.L., Pessenda, L.C.R., França, M.C., Guimarães, J.T.F., Rossetti, D.F., Lara, R.J., 2011. Holocene coastal vegetation changes at the mouth of the Amazon River. Rev. Palaeobot. Palynol. 168, 21–30. https://doi.org/10.1016/j.revpalbo.2011.09.008.
Souza-Filho, P.W.M., Lessa, G.C., Cohen, M.C.L., Costa, F.R., Lara, R.J., 2009. The Subsiding Macrotidal Barrier Estuarine System of the Eastern Amazon Coast, Northern Brazil. Lect. Notes Earth Sci. 107, 347–375. https://doi.org/10.1007/978-3-540-44771-9_11.
Spalding, M., Kainuma, M., Collins, L., 2010. World Atlas of Mangroves 319.
Suguio, K., Barreto, A.M.F., Oliveira, P.E. de, Bezerra, F.H.R., Vilela, M.C.S.H., 2013. Indicadores de variações holocênicas do nível do mar ao longo da costa dos estados de Pernambuco e Paraíba, Brasil. Geologia USP. Série Científica 13, 141–152. https://doi.org/10.5327/Z1519-874X201300040008.
Tatumi, S.H., Silva, L.P. da, Pires, E.L., Rossetti, D.F., Góes, A.M., Munita, C.S., 2008. Datação de Sedimentos Pós-Barreiras no Norte do Brasil: implicações paleogeográficas. Rev. Bras. Geociencias 38, 514–524. https://doi.org/10.25249/0375-7536.2008383514524.
Thampanya, U., 2006. Mangroves and sediment dynamics along the coasts of Southern Thailandd. Dissertation. URL. https://edepot.wur.nl/39452. (Accessed 30 December 2021).
Thornton, S.F., McManus, J., 1994. Application of Organic Carbon and Nitrogen Stable Isotope and C/N Ratios as Source Indicators of Organic Matter Provenance in Estuarine Systems: Evidence from the Tay Estuary, Scotland. Estuarine. Coastal and Shelf Science 38, 219–233. https://doi.org/10.1006/ecss.1994.1015.
Toledo, M.B., Bush, M.B., 2008. Vegetation and hydrology changes in Eastern Amazonia inferred from a pollen record. An Acad. Bras Ciências 80, 191–203. https://doi.org/10.1590/S0001-37652008000100014.
Tomazelli, L.J., 1990. Contribuição ao estudo dos sistemas deposicionais Holocênicos do Nordeste da Província Costeira do Rio Grande do Sul, com Ênfase no Sistema Eólico. PhD thesis, Porto Alegre. Universidade Federal do Rio Grande do Sul, p. 270.
Toorman, E.A., Anthony, E., Augustinus, P.G.E.F., Gardel, A., Gratiot, N., Homenauth, O., Huybrechts, N., Monbaliu, J., Moseley, K., Naipal, S., 2018. Interaction of Mangroves, Coastal Hydrodynamics, and Morphodynamics Along the Coastal Fringes of the Guianas. Coastal Research Library 25, 429–473. https://doi.org/10.1007/978-3-319-73016-5_20.
Tossou, M.G., Akoègninou, A., Ballouche, A., Sowunmi, M.A., Akpagana, K., 2008. The history of the mangrove vegetation in Benin during the Holocene a palynological study. J. Afr. Earth Sci. 52, 45167–45174. https://doi.org/10.1016/J.jafrearsci.2008.07.007.
Vedel, V., Behling, H., Cohen, M., Lara, R., 2006. Holocene mangrove dynamics and sea-level changes in northern Brazil, inferences from the Taperebal core in northeastern Pará State. Veg. Hist. Archaeobotany 15, 115–123. https://doi.org/10.1007/s00334-005-0023-9.
Walker, R.G., 1992. Facies, facies models and modern stratigrahic concepts. In: Walker, R.G., James, N.P. (Eds.), Facies Models – Response to Sea Level Change. Geological Association of Canada, Ontario, pp. 1–14.
Wolanski, E., Elliott, M., 2015. Estuarine Ecohydrology: An Introduction. In: second ed. Estuarine Ecohydrology: an Introduction Second Edition 1–321.
Woodroffe, C.D., Grindrod, J., 1991. Mangrove Biogeography: The Role of Quaternary Environmental and Sea-Level Change. J. Biogeogr. 18, 479. https://doi.org/10.2307/2845685.
Yao, Q., Liu, K.B., 2017. Dynamics of marsh-mangrove ecotone since the mid-Holocene: A palynological study of mangrove encroachment and sea level rise in the Shark River Estuary, Florida. PLoS One 12, e0173670. https://doi.org/10.1371/journal.pone.0173670.